AFRL-VS-TR-2003-1593

VALIDATION OF IONOSPHERIC MODELS

Patricia Doherty

Boston College
Institute for Scientific Research
140 Commonwealth Avenue
Chestnut Hill, MA 02467-3862

31 March 2002

Scientific Report No. 6

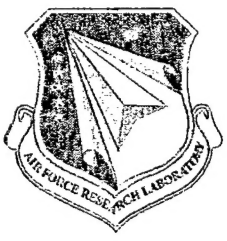

AIR FORCE RESEARCH LABORATORY
Space Vehicles Directorate
29 Randolph Rd
AIR FORCE MATERIEL COMMAND
Hanscom AFB, MA 01731-3010

"This technical report has been reviewed and is approved for publication"

/signed/

JOHN RETTERER
Contract Manager

/signed/

ROBERT MORRIS
Branch Chief

This report has been reviewed by the ESC Public Affairs Office (PA) and is releasable to the National Technical Information Service (NTIS).

Qualified requestors may obtain additional copies from the Defense Technical Information Center (DTIC). All others should apply to the National Technical Information Service (NTIS).

If your address has changed, if you wish to be removed from the mailing list, or if the addressee is no longer employed by your organization, please notify AFRL/VSIM, 29 Randolph Road, Hanscom AFB MA 01731-3010. This will assist us in maintaining a current mailing list.

Do not return copies of this report unless contractual obligations or notices on a specific document require that it be returned.

REPORT DOCUMENTATION PAGE

Form Approved
OMB No. 0704-0188

1. REPORT DATE *(DD-MM-YYYY)*	2. REPORT TYPE	3. DATES COVERED *(From - To)*
31-03-2002	Scientific Report No. 6	April 2001 - March 2002

4. TITLE AND SUBTITLE

VALIDATION OF IONOSPHERIC MODELS

5a. CONTRACT NUMBER
F19628-96-C-0039

5b. GRANT NUMBER

5c. PROGRAM ELEMENT NUMBER
61102F

6. AUTHOR(S)

Patricia H. Doherty

5d. PROJECT NUMBER
1010

5e. TASK NUMBER
IM

5f. WORK UNIT NUMBER
AC

7. PERFORMING ORGANIZATION NAME(S) AND ADDRESS(ES)

Boston College / Institute for Scientific Research
140 Commonwealth Avenue
Chestnut Hill, MA 02467-3862

8. PERFORMING ORGANIZATION REPORT NUMBER

9. SPONSORING/MONITORING AGENCY NAME(S) AND ADDRESS(ES)

Air Force Research Laboratory (VSBP)
29 Randolph Road
Hanscom AFB, MA 01731-3010

10. SPONSOR/MONITOR'S ACRONYM(S)

11. SPONSOR/MONITOR'S REPORT NUMBER(S)
AFRL-VS-TR-2003-1593

12. DISTRIBUTION/AVAILABILITY STATEMENT

Approved for public release; distribution unlimited.

13. SUPPLEMENTARY NOTES

14. ABSTRACT

During the period of April 2001 through March 2002, we have continued to pursue the validation of ionospheric models. These efforts included the development of software to enable assimilation of new data types into the Parameterized Real-Time Ionospheric Specification Model (PRISM). This work required validation of the output from the enhanced PRISM input. Other validation efforts included analysis of the Total Electron Content (TEC) generated by the PRISM model and determination of the accuracy of the GPS Positioning Error Maps that are part of the OPerational Space Environment Network Display (OP-SEND). The Coupled Ionospheric Thermosphere Electrodynamic Forecast Model was enhanced by adding the Thermosphere Forecast Model. Ionospheric response to geomagnetic storms was also a focus of our work in the current year together with the development of automated software to perform quality control of ionogram data. The work summarized above resulted in seven presentations at various ionospheric conferences and one published journal article. The journal article is appended to this report.

15. SUBJECT TERMS

Ionosphere, Parameterized Real-time Ionospheric Specification Model (PRISM), Special Sensor Ultraviolet Limb Imager (SSULI), Special Sensor Ultraviolet Spectrographic Imager (SSUSI), Coupled Ionosphere Thermosphere Electrodynamic Forecast Model (CITEFM), Global Positioning System (GPS), Position Errors, OPerational Space Environment Network Display (OP-SEND)

16. SECURITY CLASSIFICATION OF:			17. LIMITATION OF ABSTRACT	18. NUMBER OF PAGES	19a. NAME OF RESPONSIBLE PERSON
a. REPORT	b. ABSTRACT	c. THIS PAGE			John Retterer
U	U	U	SAR		19b. TELEPHONE NUMBER *(Include area code)* 781-377-3891

TABLE OF CONTENTS

LIST OF FIGURES

1. GOALS

The objective of this contract is to obtain ionospheric measurements from a wide range of geographic locations and to utilize the resulting databases to validate the theoretical ionospheric models that are the basis of the Parameterized Ionospheric Specification Model (PRISM) and the Ionospheric Forecast Model (IFM).

In this past year, we have supported these goals with the following activities:

- Enhanced software to pre-process data for input to PRISM.
- Performed validations of the PRISM model.
- Performed validations of the Global Positioning System (GPS) Single-Frequency Position Error Maps.
- Supported model development for the Communication and Navigation Outage Forecast System (C/NOFS).
- Analyzed ionospheric response to geomagnetic storm activity.
- Developed automated software to perform quality control and modification of ionogram data.

2. PROGRESS

2.1 UltraViolet (UV) PRISM Pre-processor

In the current year, much progress was made in the development of technology to integrate environmental parameters derived from UV sensors as part of PRISM's near real-time data input.

Two UV sensors are under development for the DMSP Block 5D-3 satellites. Both are remote-sensing instruments that measure UV emissions emitted by the Earth's upper atmosphere. One instrument is the Special Sensor Ultraviolet Limb Imager (SSULI), which scans the limb of the Earth in the orbital plane. The other instrument is the Special Sensor Ultraviolet Spectrographic Imager (SSUSI), which measures emissions in five different wavelength bands. The resultant images cover the visible Earth disk from horizon to horizon and the anti-sunward limb up to an altitude of approximately 520 km.

These sensors have the potential to significantly improve ionospheric remote sensing. To take advantage of this opportunity, the data from these new sensors must be able to be used by operational products. Modifying PRISM to accept new data types is a difficult and time-consuming task. Therefore, we have developed software techniques that will accept the DMSP UV sensor data, extract the relevant data and convert it into a data type currently accepted by PRISM. This software is called UV PRISM. Work described in last year's annual report resulted in PRISM revisions that allowed a great number of data inputs.

In the current year, we have completed development of the first and second version of the UV PRISM product and have generated scenarios of the UV data as input to PRISM. We have also defined the potential benefit of the UV data to near real-time ionospheric specification with PRISM.

The UV PRISM pre-processor, which is named PRISM Data Preprocessor (PDP), has been written in Fortran. This language was chosen to keep the entire PRISM package, the PDP and PRISM itself, in a common language. The PDP reads the standard PRISM input files, the SSULI and SSUSI data, and creates PRISM input files that contain both UV and data from the other sources. PDP development resulted in several versions with each version adding the capability for more complexity in the processing and assimilation of UV data.

As part of the development of the UV PRISM pre-processor, significant testing was performed. This included robustness tests and simulated assessment of UV-PRISM errors. The robustness tests were designed to affirm that the PDP was working as designed and that PRISM reproduced the UV data correctly. The simulated assessment of UV-PRISM errors was designed to assess the potential benefit of using UV data in PRISM. Given that this work was completed before any SSUSI or SSULI data was available, we had to simulate measurements of the data to test the software.

The simulations of the UV data were based on a model ionosphere. From the model ionosphere, we calculated the quantities that will be observed or inferred by the UV observations. To accomplish this, we used the International Reference Ionosphere (IRI) model. This model was selected because we have found, in previous work, that the IRI and PRISM climatology can have significant differences for the same geophysical conditions. A simulated data set was created by selecting a date, a UT time, a set of geophysical conditions and a satellite track. Figure 1 shows the pixel locations of the simulated UV measurements covering the hours of 10-14 UT on January 2, 2000 for the F15 DMSP satellite track. The plot is color coded to represent the different types of measurements. The DMSP track is plotted with a solid black line. The SSUSI day disk pixels are plotted in red. The SSUSI night disk pixels are plotted in blue. The day and night limb pixels are in purple. The auroral pixels are in yellow. The locations of the SSULI measurements are plotted near the DMSP track in green. For display, we have included the locations of twilight pixels in black. Note that no UV data are simulated for these twilight pixels.

As can be seen, for SSULI the data are produced essentially in track either ahead or behind the satellite depending on how the instrument is mounted and how the satellite is oriented. In this simulation, we assumed the instrument is scanning behind the satellite producing a profile every 120 seconds (green dots). SUSSI, on the other hand, produces data along a cross track scan and on the limb to the anti-sunward side. The different regions are defined by evaluating the solar zenith angle at each pixel location. Twilight is defined to be that region where the solar zenith angle is between 90-110 degrees. For that region, no simulations are made (black dots) for either SSUSI or SSULI. The auroral pixels are for an arbitrary chosen latitude band at high latitudes that is not in twilight. We

assume there is a scan of SSUSI parameters every 60 seconds. The three tracks going over the Western Hemisphere are the morning passes and the two tracks crossing Asia are the evening passes.

Several simulated tests using different times, seasons and geophysical conditions were run to determine the impact of using TEC derived from SSUSI and SSULI as input to PRISM. The simulations were generated with a series of programs that produce the simulated data using IRI along the DMSP F15 satellite track. The programs are named: makeUVtracks.for and UV_IRI2001.for. Results of using the simulated data in PRISM directed further study to define methods of data quality control and improved procedures for merging satellite and ground-based data sets. These efforts will continue into the next year of this contract.

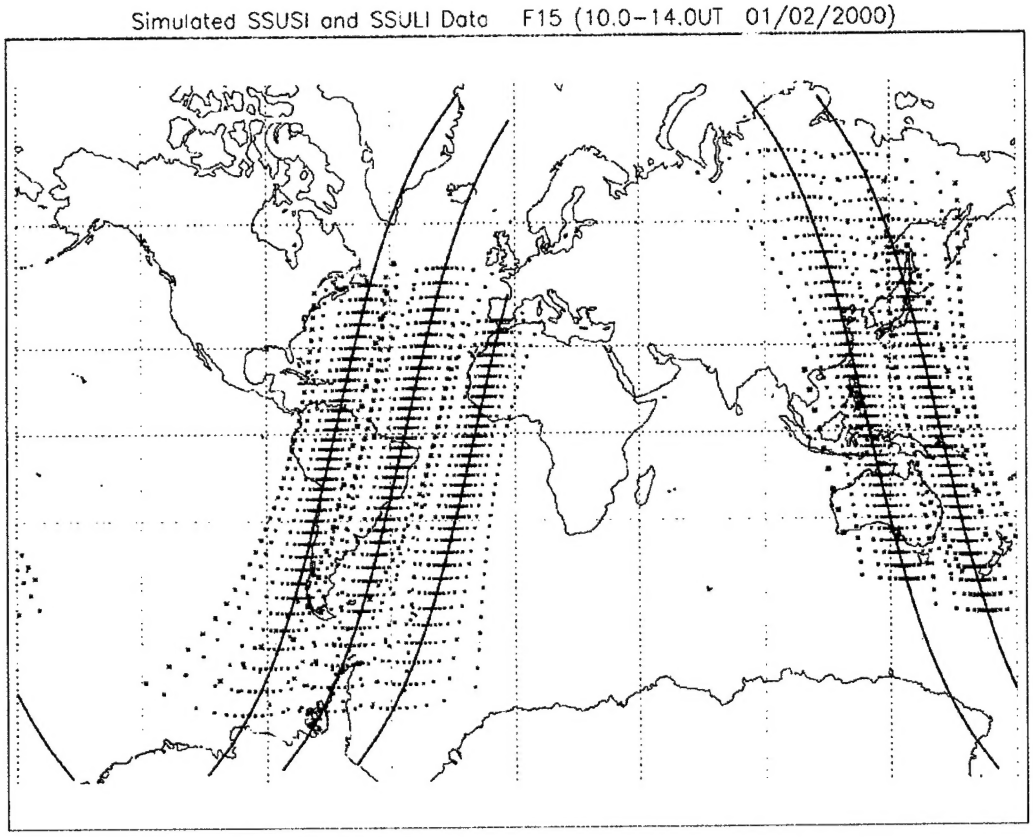

Figure 1. Pixels Locations of Simulated SSUSI and SSULI Data Using DMSP Track F15 on 1/2/2000 Between 10 and 14UT.

2.2 PRISM Model Validations

Work was initiated to determine the accuracy with which PRISM can predict the TEC on oblique satellite paths to a single station as well as the difference of the TEC's on two satellites observed at one ground station.

The accuracy of the GPS position solution is dependant on the difference in TEC between the lines of sight to pairs of satellites, rather than on the absolute values. The accuracy of space-based geolocation systems has a similar dependence. In our work this year, we have attempted to define PRISM's ability to improve the accuracy of absolute TEC predictions, rather than TEC differences, since these preliminary studies would help to provide explanations of the errors in the calculated differences. The overall plan was to run PRISM in its Real Time Adjustment (RTA) mode, using the TEC values for approximately 30 IGS stations that are now provided to AFRL in near real time by JPL. A small number of stations were set aside for use as ground-truth stations, while the rest were used as drivers to be used by PRISM to update its climatological model. The general aim of the project was not achieved due to lack of suitable TEC data. The basic problem was that the stations were too few and too far apart, except for the ten North American stations, for which RTA PRISM provided substantial improvements over its climatological model (CLM).

Problems also arose because of calibration errors in the JPL values of TEC. Three of the thirty stations, for which data were provided, were found to have large offsets. For example, the PIMO (Phillipines) were 46 TECU too high. Errors such as this prevent RTA PRISM from achieving improvements over the CLM results. These offsets showed up in the monthly median values of observed vertical TEC at a station that were derived by a new technique.

The results of our efforts in this project are that the accuracy of PRISM RTA TEC values clearly cannot be tested definitively until errors in the observed TECs are identified and removed. In other words, Quality Control procedures (preferably automatic) need to be developed, and applied to the real-time data before it is passed to PRISM. This work will be addressed in the next year of this contract.

Techniques have been developed to control the operation of PRISM by Unix scripts, and several analysis programs have been written in Fortran. The International Reference Ionosphere (IRI) has been incorporated into the analyses to act as a straw man, since any real-time ionospheric model must be more reliable than the empirical IRI. The accuracy of the IRI predictions is also useful information for the COSPAR IRI working Group. Two internal technical reports were produced to describe the results of this effort. These reports are summarized below:

"Comparison of PRISM Values of Slant TEC with JPL Observation," February 2002

Summary: The hourly values of Total Electron Content (TEC) derived at three ground stations by the Jet Propulsion Laboratory (JPL) from observations of GPS satellites in January 2002 have been analyzed, as part of a continuing AFRL effort to validate the PRISM ionospheric model. Calculations of the PRISM values of slant TEC for the three stations have been compared with the observations.

The three stations (Fort Davis, Texas, Easter Island and Guam) are taken as "ground-truth" stations, while observations at the other 26 stations have been used as "driver" stations. When run in its real-time assimilation (RTA) mode, PRISM assimilates the "observed" equivalent vertical TECs at all ionospheric pierce points for a particular time, forcing the ionospheric model to reproduce the observations as well as possible. When no real-time observations are available, PRISM reverts to a climatological model (CLM).

The errors are found to have a strong local-time dependence, so all comparisons made for each universal time are associated with the corresponding local time at the observing station. The present analysis uses several error metrics to show the errors for both the RTA and CLM approaches, and to illustrate the significant decrease in error between the two approaches.

During the day at a midlatitude site in west Texas (Fort Davis) that is close to several driver stations (the ideal case), the RMS RTA errors are a factor of two to five times smaller than the CLM errors, and comparable to the uncertainties in the observed values. The relative accuracy of the RTA results versus the CLM results is generally lowest at night.

For the other two ground-truth stations, Easter Island (Chile) and Guam, the driver stations are all too far away to provide any data that is particularly useful for assimilations, although the RTA errors are marginally less than the CLM errors during the day.

The study reported here will be continued as more TEC observations become available.

"Derivation of Monthly Median Values of Vertical Incidence TEC at IGS Ground Station," April 2002

Summary: The hourly values of Total Electron Content (TEC) derived at 30 International GPS Service (IGS) ground stations by the Jet Propulsion Laboratory (JPL) from observations of GPS satellites are routinely sent to AFRL. These observations correspond to the TEC along the lines of sight (LOS) to multiple satellites.

As such, these observations are exactly what are required for studies concerned with the ability of ionospheric models to predict the TEC along the LOS to a GPS satellite (i.e., the slant TEC) in operational situations, when observations of the TEC are not available. Values of slant TEC provide very stringent tests of an ionospheric model, because the LOS covers a range of latitudes and longitudes, as well as height. Thus, both the local N (h) profile and the horizontal ionospheric gradients must be well modeled. However, these slant TEC observations are less than ideal for workers who are attempting to validate and improve current ionospheric models, or to develop new ones. In this case, and at this stage of model development, the preferred input is the vertical TEC, i.e., the TEC for a vertical path at a station. Values of the vertical TEC have historically been derived by using the simple cos χ formula to relate the observed slant TEC to the (equivalent) vertical TEC corresponding to the ionospheric pierce point (IPP). The IPP is

simply the sub-satellite location for the point at which the LOS passes through a particular altitude. This altitude is usually taken to be about 400 km. For example, JPL uses an altitude of 450 km to determine the IPPs and the vertical TEC from the GPS observations.

It is well known that the simple cos χ conversion can introduce significant errors into the supposed vertical TEC. What is more, the IPPs move around as the satellites move, so the vertical TECs obtained in this way are of limited direct use to the ionospheric modeler.

This paper describes a method for deriving the monthly median values of the vertical TEC at any IGS site. The method is completely mathematical, and makes no physical assumptions akin to the simple cos χ conversion procedure. The basic procedure is to determine the asymptotic limit of the TEC as a function of elevation angle, as the elevation angle goes to 90 degrees, which corresponds to the vertical TEC for the IGS station. The limit for each hour is determined in a least-squares fit procedure, and then the 24 hourly values of the 90 degrees limit are smoothed by a similar procedure. A least-squares procedure is made mandatory by the small sample sizes.

Illustrative examples are presented, along with analyses that verify the reliability and illustrate the utility of the derived medians. The error bars can be quite large at times, because of the small sample sizes. However, until the ionospheric models improve substantially, the accuracy of the derived monthly values is more than sufficient for testing them.

2.3 Validation of the GPS Single Frequency GPS Error Maps

In this current year, we have continued efforts to validate the OpSend Estimated Single-Frequency GPS Position Error Maps that are produced operationally for the 55th Space Weather Air Force Group. These maps estimate the position errors that result from inaccurate ionospheric corrections for the GPS single-frequency user. The original software that produces these maps of position errors was developed in an earlier period of this contract. It determines the errors by using the slant total electron content (TEC) from the PRISM model. The utility of these maps is highly dependent on the accuracy of PRISM and the fact that the error budget for single-frequency determined positions is dominated by the range delay caused by the ionosphere. A typical figure produced by the OpSend Estimated GPS Single-Frequency Position Error Map is shown in Figure 2. Note that the contours of the estimated position errors are plotted in color according to the color bar on the right side of the maps.

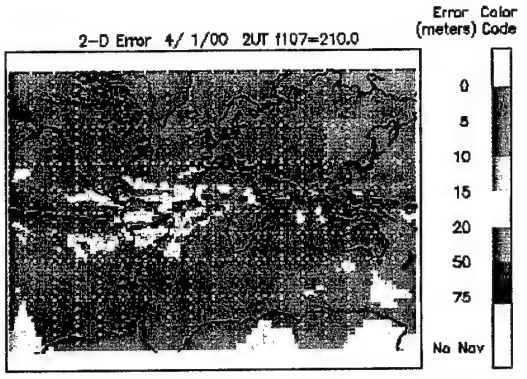

Figure 2. Typical OpSend Estimated GPS Single-Frequency Position Error Map.

This year, we completed validation for the maps with data recorded at Ascension Island in March-April 2000. Ascension Island is located within proximity of the south atlantic equatorial anomaly region. This region experiences the highest magnitudes in electron content together with frequent and significant periods of ionospheric scintillation. It presented the most challenging case for use and validation of the Position Error Maps.

To complete the validations and automate the validation procedure, a master program was written to perform the entire process in an automated method. The program was written in the IDL language and is named "run_val.pro." The procedure is comprehensive in that, for every single-frequency measurement at 5-minute intervals, it runs the entire process – from running PRISM to calculating and plotting the 2 and 3 dimension position errors. Details of this process are described in Quarterly Report 23.

In Figure 3 we show results of validation at Ascension Island for March 24, 2000. The top panel shows the Dilution of Precision (GDOP) (black for what was reported by single-frequency receiver, red for the flat option of product generator, and blue for hilly option of product generator). The flat option indicates that all satellite line-of-sight data above 5 degrees elevation angle from the station was used in the calculations. The hilly option limits usable data to satellite lines of sight above 15 degrees elevation. The middle panel gives the 2-dimension (2D) position error from the observations (black), the flat option of the product generator (red), and the hilly option of the product generator (blue). The bottom panel similarly gives the 3-dimension (3D) position error.

We see that in the GDOP plot the flat results look fairly similar to the receiver produced GDOP. The hilly option clearly produced some significantly different GDOPs. On the other hand, in the 2D error it is the hilly option that appears to follow the observations more closely as compared to the flat option. The one exception is in the evening where the flat option does a bit better at capturing the strong variations in the observations. However, in general, while the product generator is producing structure that is suggestive of what is observed clearly there are significant differences in the details of the structure. One major feature in Figure 3 is the large GDOP value that occurs for the hilly case between 3 and 4 UT. Large GDOPs are the result of poor satellite geometry. In general, large GDOPs will increase position errors; however, in this case the hilly 2D and 3D

position errors are relatively small. Determining the exact cause for this anomalous behavior should be pursued, but it was beyond the scope of this study.

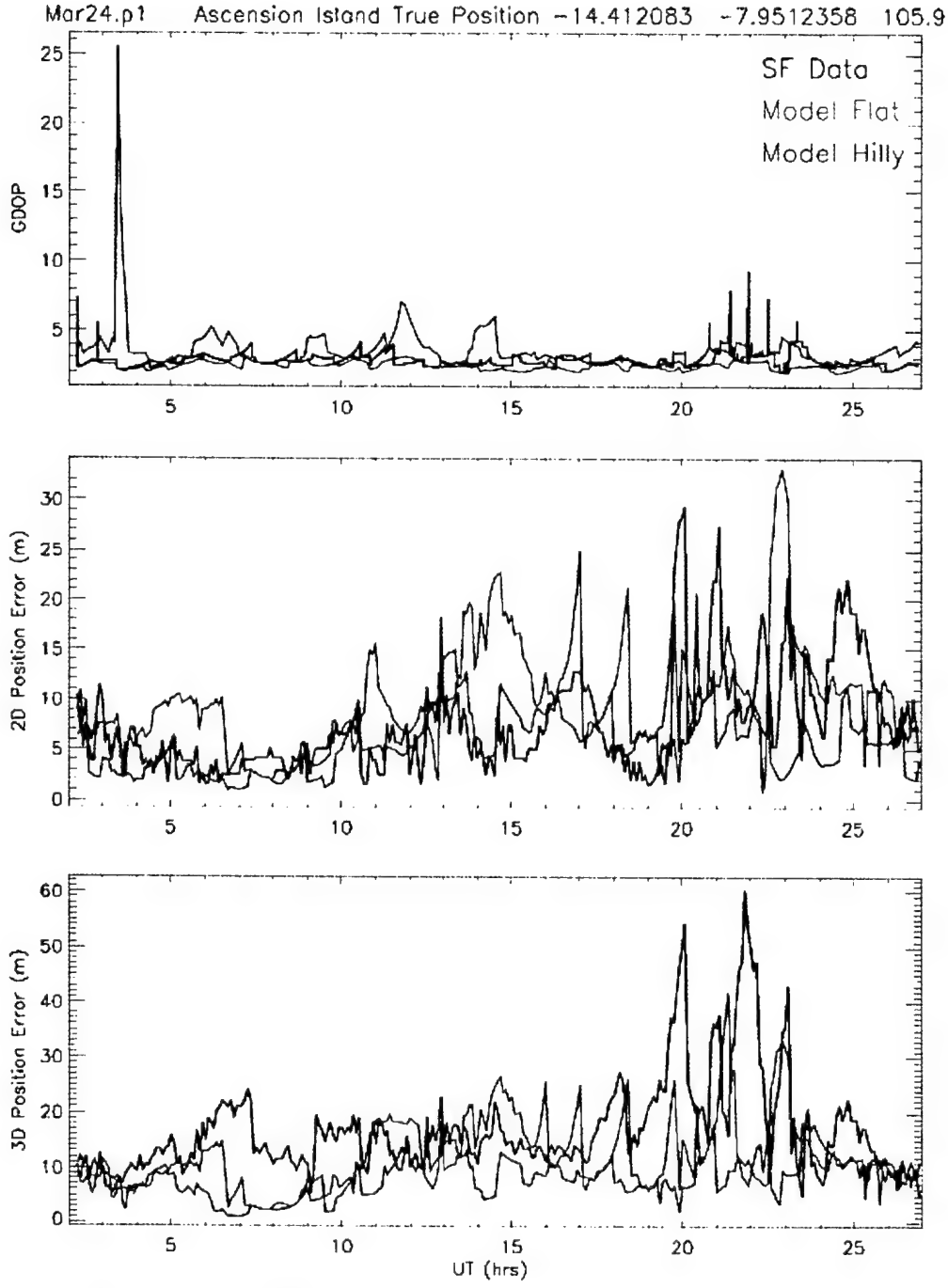

Figure 3. Comparison of Observed and Estimated Quantities for March 24 2000 at Ascension Island. Top panel gives GDOP. Middle panel gives 2D position errors and bottom panel gives 3D position errors. All quantities are given at 5-minute resolution.

A similar conclusion can be made for the 3D error. However, we do see some interesting differences with the 2D results. In the early daylight (5 – 10 UT) both the flat and hilly option for the 3D error significantly underestimates the observed error. Further, both the flat and hilly don't capture the full magnitude of the observed early evening variability.

To provide a view that doesn't get lost in all the detailed structure of Figure 3, in Figure 4 we have smoothed the product generator results by using a polynomial fit. Here the organization of the plots is the same as in Figure 3. We can see that for around the first 10 hours of the day the flat and hilly smoothed results bracket much of the observed 2D error. Later in the day the variability clearly does not stay contained within the smoothed flat and hilly results. In the 3D results, there is really no region where you can say the flat and hilly results bracket the observations. In the early daytime (5 – 9 UT) both product generator results clearly underestimate the observations. In summary, for 2D errors the hilly smooth result does the better job at capturing the baseline observed behavior. For the 3D error, it is the smoothed flat result that does a bit better at describing the observed baseline behavior. However, a smoothed result obviously misses an important feature of the observations, that is the large variability especially in the early evening.

Another view of what is happening in detail is given in Figure 5 where we show the differences between the observed and modeled errors. The middle panel reinforces what was seen in Figure 3 for the 2D error. For the first half of the day the hilly results hover around zero difference with the observations. Approaching and during the evening both the flat and hilly results show large differences with observations. In some cases the flat and hilly show similar results, in other cases, they show dramatic differences. In the 3D error, we can see the sizeable underestimation in both the flat and hilly results for early daytime (5 – 9 UT) as well as the large differences in the evening.

Given the great variability in the data as well as in the product generator results, we decided to make comparisons averaged over time. In particular, we averaged the 5 minute results over an hour. In Figure 6, we give the hourly means and standard deviations of the difference between the estimated and measured error. Thus, each average and standard deviation shown is based on 12 points. The top panel is the 2D error difference using the flat results. The next panel shows the same parameters for hilly terrain. The bottom two panels illustrate the results for the 3D cases. We can see the features that were evident in the preceding more detailed plots. In the second panel, we see the hilly results giving differences within 3 meters for the first half of the day. The average difference for 13 to 14 UT gets up to around 4 meters, but it is after 20 UT (evening) that we see the largest errors (up to 10 meters). Again, in the 3D error we see the underestimation by both flat and hilly results that peaks around 7 UT as well as the large differences in the evening.

These figures were produced for the full 14-day period of the Ascension Island data set. Results were fairly consistent with the results presented in Figures 3 through 6 for March 24, 2000. A full summary of the results was prepared for a report to the Air Force. This report will be finalized in the next year of this contract.

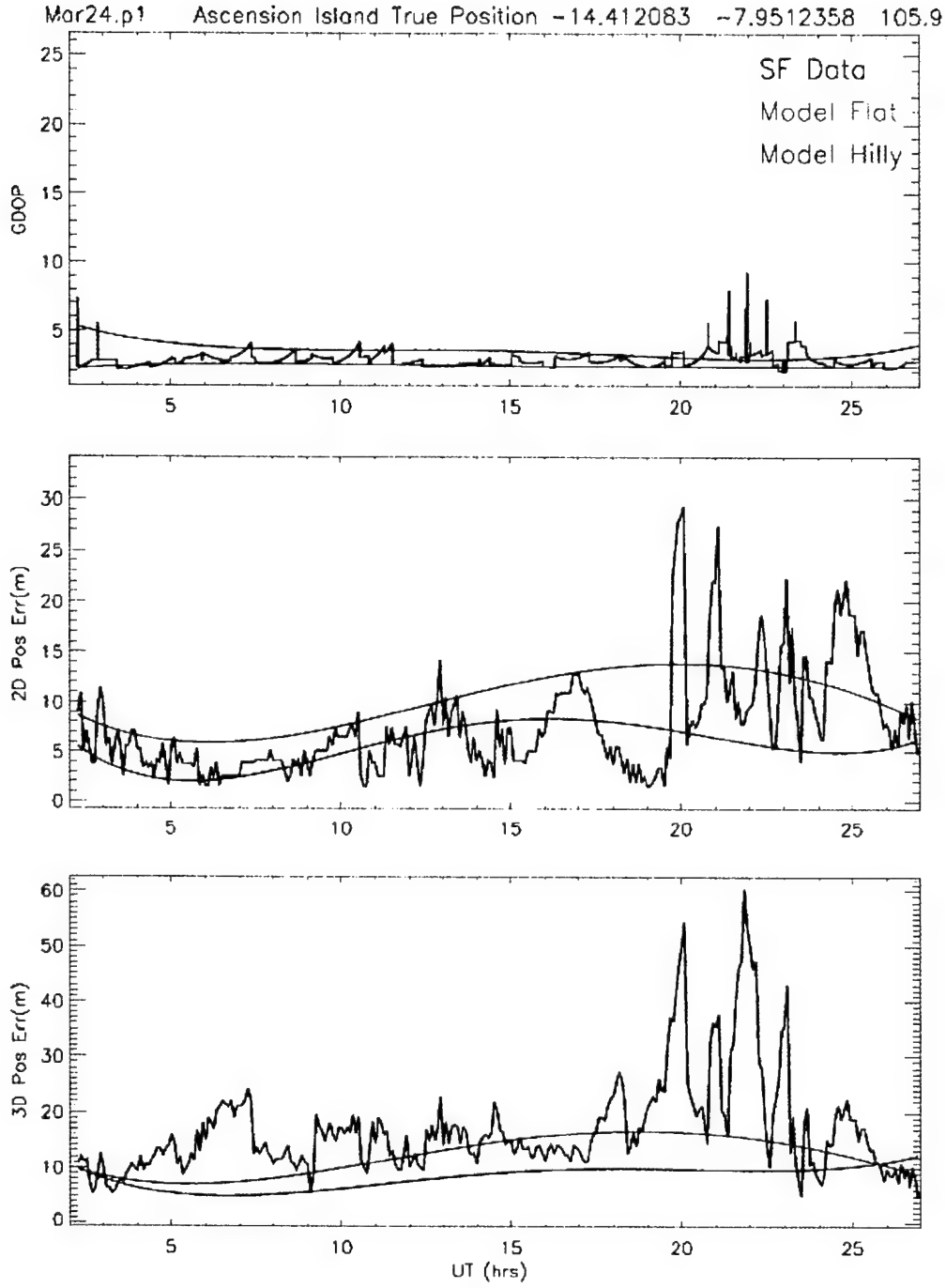

Figure 4. Comparison of Observed and Estimated Quantities for March 24 2000 at Ascension Island. Top panel gives GDOP. Middle panel gives 2 dimension position errors and bottom panel gives 3 dimension position errors. The estimated quantities have been smoothed using a fourth order polynomial fit.

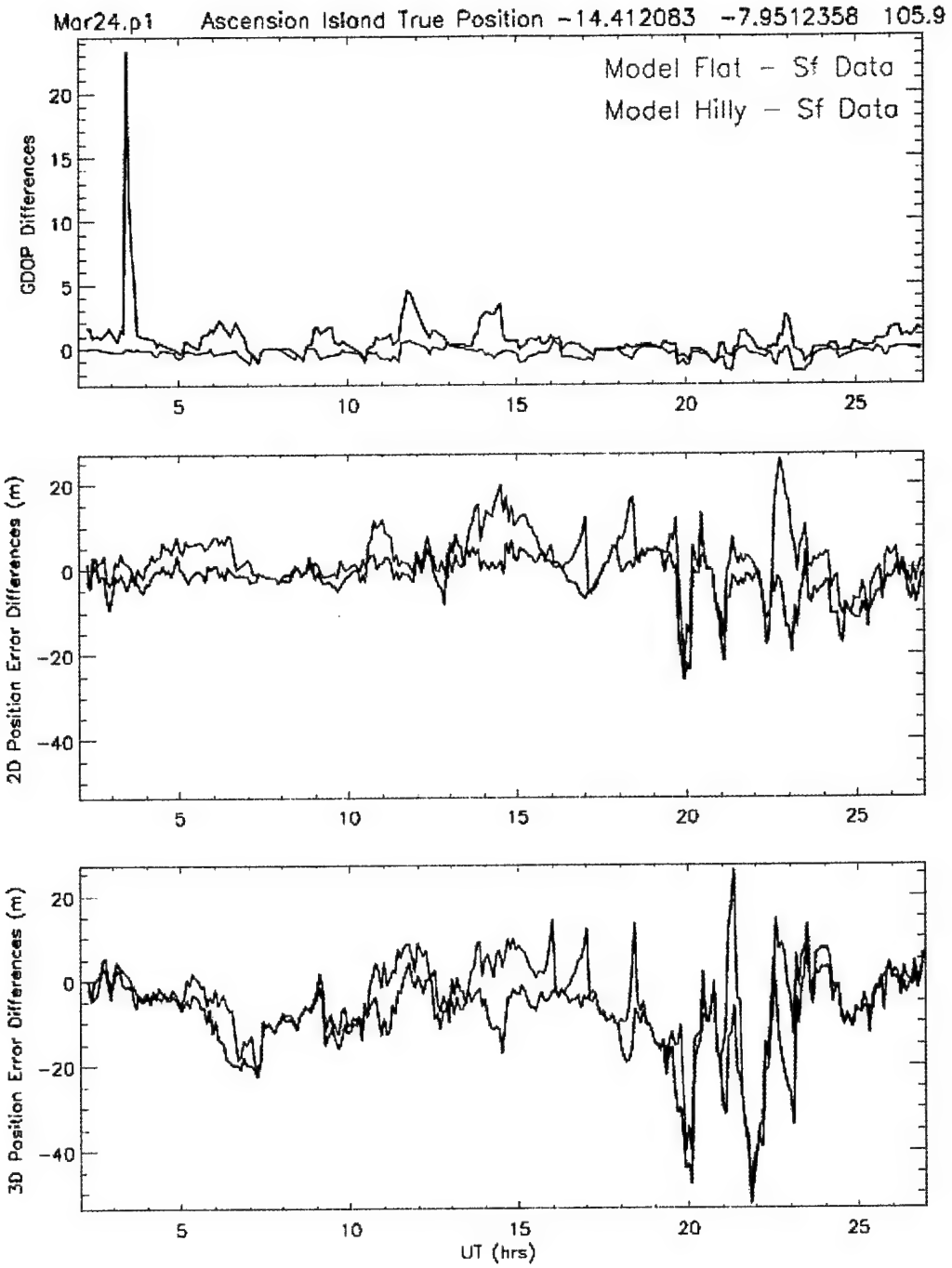

Figure 5. Plots of Differences Between Observed Quantities and the Product Generated Quantities for March 24 2000 at Ascension Island. Top panel gives GDOP difference. Middle panel gives differences in the 2 dimension position errors and bottom panel gives differences in 3 dimension position errors.

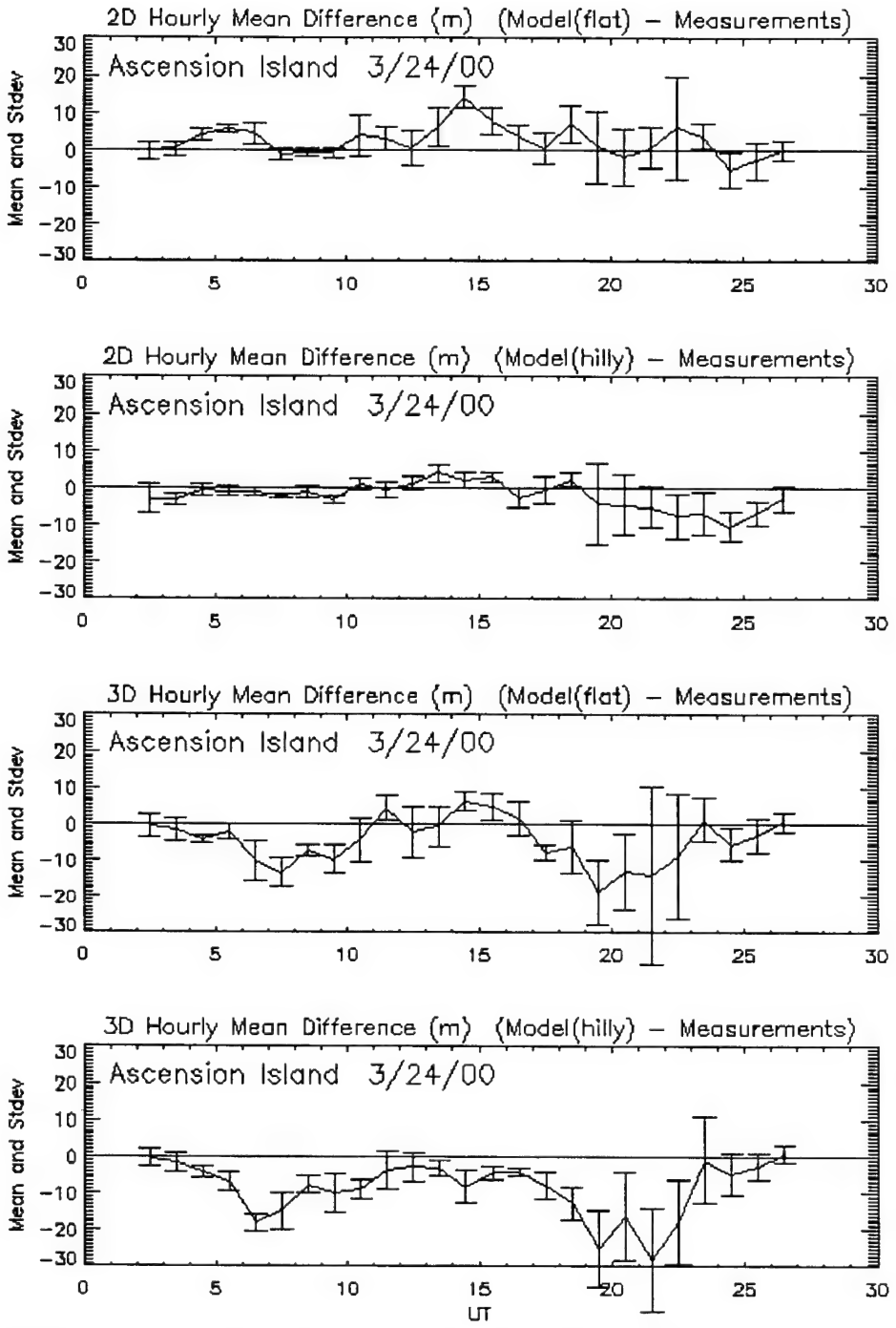

Figure 6. The Mean Hourly Difference for March 24 2000 Between Model and Measurements. It is the mean of the differences over 1 hour's time (i.e. 12 values averaged). The error bars are the standard deviations over those 12 differences. The top panel gives the differences between product with the flat option and the observations for the 2-dimension position error. The second panel is for the hilly option for the 2D case. The third panel shows the differences for the 3-dimension error using the flat option. The bottom panel has the 3D differences using the hilly option of the product generator.

2.4 C/NOFS Modeling Efforts

Graphics development to animate and illustrate the models for C/NOFS were completed in the last fiscal year and transferred to AFRL at the beginning of the current year. In addition, further efforts were made to modify the CITEFM model to include a thermosphere model (TFM) in the code. Significant time was spent validating and improving the coupling of TFM into CITEFM. As a result, modifications and improvements were made to CITEFM. This work continues into the next year.

2.5 Ionospheric Storm Studies

In last year's annual report, we described a study of one of the most significant ionospheric storms of the current solar cycle. That storm occurred in July 2000. In the current year, we have continued our effort to utilize GPS TEC measurements to determine the particular complexities of this storm period. Results of that work were presented at two Space Weather Workshops.

In addition to work on the July 2000 storm, we participated in a study of storm activity during the International Space Weather Period of September and October 1999. This study included GPS observations, VHF/UHF scintillations, and in situ density structures at middle and equatorial latitudes. The overall conclusion of this study was that the prompt penetration of magnetospheric electric fields caused TEC increases, followed by rapid TEC decreases related to the equatorward motion of the midlatitude trough. These effects were enhanced if the rapid Dst storm index intensifications took place in the afternoon sector near dusk. The equatorward motion of the trough was accompanied by TEC fluctuations, some as large as 5 TEC units, and saturated 250MHz scintillations, which may impact a GPS-based navigation system such as the Wide Area Augmentation System (WAAS) and UHF communication links.

The results of this work were presented at a Space Weather Conference. They were also published in Radio Science.

2.6 Quality Control and Modfication of Ionogram Data

A program was developed to perform quality control scans, modifications and excisions for Digisonde ionogram data that has been obtained by the auto-scaling program ARTIST. QualCon is an expert automated system similar to ARTIST. QualCon was developed in response to known deficiencies in the ARTIST program. ARTIST was found to poorly scale ionograms from sites with forbidden frequency bands. QualCon picks up most of the incorrect scalings by application of a series of tests. A detailed report on the development of QualCon was prepared and submitted to AFRL in the current year.

3. PRESENTATIONS

Basu, S., Basu, Su., Valladares, C.E., Aarons, J., Doherty, P., and Groves, K., "Ionospheric Effects of Major Magnetic Storms During the International Space Weather Period of September and October 1999: GPS Observations and VHF/UHF Scintillations at Middle and Equatorial Latitudes," presented to the International Workshop on Space Weather Effects held in Boston, MA in June 2001.

Beaujardiere, O. D., Decker, D.T., Borer, W., Retterer, J., Bullett, T., Bishop, G., Groves, K., Jeong, L., and Doherty, P., "Future Directions in Ionospheric Space Weather Application," presented as an invited talk to the Fall AGU 2001 Meeting, held in San Francisco, CA in December 2001.

Bishop, G., Quigley, S., Groves, K., Bullet, T., Doherty, P., Sexton, E., Citrone, P., Scro, K., and Wilkes, K., "Operational Space Weather Impact Maps for RF Systems," presented to the International Workshop on Space Weather Effects held in Boston, MA in June 2001.

Doherty, P.H., Klobuchar, J.A., and Delay, S.H., "The Great Ionospheric Storm of July 2000: GPS Measurements and System Effects," presented at the Space Weather Workshop held in Boulder, CO in May 2001.

Doherty, P.H., Klobuchar, J.A., and Delay, S.H., "Ionospheric Response to the Great Storm of July 2000," presented at the International Workshop on Space Weather Effects held in Boston, MA in June 2001.

Doherty, P.H., Klobuchar, J.A., Delay, S.H., and Valladares, C.E., "Ionospheric Scintillation Effects on WAAS Receivers in the Auroral and Near-Equatorial Regions," presented at the International Beacon Satellite Symposium held in Boston, MA in June 2001.

Pulliam, R., Borer, W., Decker, D.T., and Doherty, P.H., "PRISM Validation Study," presented to the International Workshop on Space Weather Effects held in Boston, MA in June 2001.

4. JOURNAL ARTICLES

Basu, Su., Basu, S., Valladares, C.E., Yeh, H.C., Su, S.Y., MacKenzie, E., Sultan, P.J., Aarons, J., Rich, F.J., Doherty, P.H., Grove, K.M., and Bullet, T.W., "Ionospheric effects of major magnetic storms during the international space weather period of September and October 1999: GPS observations, VHF/UHF scintillations and in-situ density structures at middle and equatorial latitudes", *Journal of Geophysical Research*, ***Vol. 106***, No. A12, Pages 30,389-30,413, December 2001. (see Appendix)

APPENDIX

JOURNAL OF GEOPHYSICAL RESEARCH, VOL. 106, NO. A12, PAGES 30,389–30,413, DECEMBER 1, 2001

Ionospheric effects of major magnetic storms during the International Space Weather Period of September and October 1999: GPS observations, VHF/UHF scintillations, and in situ density structures at middle and equatorial latitudes

Sunanda Basu,[1] Santimay Basu,[2] C. E. Valladares,[3] H.-C. Yeh,[4] S.-Y. Su,[4] E. MacKenzie,[3] P. J. Sultan,[2] J. Aarons,[5] F. J. Rich,[2] P. Doherty,[3] K. M. Groves,[2] and T. W. Bullett[2]

Abstract. In this paper we present a study of the ionospheric effects of a halo coronal mass ejection (CME) initiated on the Sun on September 20, 1999, and causing the largest magnetic storm during this month on September 22–23, 1999, with the hourly *Dst* index being −167 nT at ~2400 UT on September 22. The recurrent CME on October 18 caused an even larger magnetic storm on October 22, 1999, with *Dst* of −231 nT at ~0700 UT. The ionospheric effects of these two major magnetic storms are studied through their effects on a prototype of a Global Positioning System (GPS)-based navigation system called Wide Area Augmentation System (WAAS) being developed by the Federal Aviation Administration for use in the continental United States and their impact on global VHF/UHF communication systems. It is shown that the penetration of transient magnetospheric electric fields equatorward of the shielding region at midlatitudes, which have been well-correlated in the past with rapid changes in the well-known *Dst* index (or through its recently available high resolution 1-min counterpart the SYM-H index), can cause large increases of total electron content (TEC), TEC fluctuations, and saturated 250-MHz scintillation, and these, in turn, may have significant impacts on WAAS. The local time of *Dst* changes (and not just *Dst* magnitude) was found to be very important for WAAS, since the largest effects on TEC are seen near dusk. The prompt penetration of these magnetospheric electric fields all the way to the magnetic equator causes augmentation or inhibition of equatorial spread *F*. The global ionospheric response to these storms has been obtained from ground-based TEC observations with a GPS network and space-based in situ density and electric field measurements using the Republic of China Satellite–1 (ROCSAT-1) and several Defense Meteorological Satellite Program satellites. These prompt penetration electric fields cause VHF/UHF scintillations and GPS TEC variations at low latitudes in the specific longitude sector for which the early evening period corresponds to the time of rapid *Dst* variations and maximum *Dst* phase. The effects of the delayed ionospheric disturbance dynamo and those of decreased magnetospheric convection on postmidnight irregularity generation are shown to be confined to a part of the same longitude range that actively responded to the prompt penetration of electric fields in the early evening sector.

1. Introduction

The Solar Terrestrial Energy Program–Research, Applications and Modeling Phase (S-RAMP) Group of the Scientific Committee for Solar Terrestrial Physics (SCOSTEP) conceived and coordinated a month-long campaign interval during September 1999 as an International Space Weather Period (ISWP) to follow the progress of space weather events from their initiation on the Sun to their impacts at the Earth, including their effects on space-based and ground-based technological systems and for assessment of the accuracy of specification and forecasting techniques. A great deal of material on the geoeffective solar wind events during this month has been compiled in a special Web page for which the URL is http: \\aoss.engin.umich.edu/intl_space_weather/sramp/ to which the reader is referred for additional information (J. U. Kozyra, private communication, 1999). Here we provide some basic information on the interplanetary shocks and southward interplanetary magnetic fields (IMF) that triggered the largest magnetic storm during the core campaign period.

This large magnetic storm was triggered by an interplanetary magnetic cloud (IMC) event extending from 2000 UT on September 22 to 0700 UT on September 23 with maximum IMF >

[1]Atmospheric Sciences Division, National Science Foundation, Arlington, Virginia, USA.
[2]Space Vehicles Directorate, Air Force Research Laboratory, Hanscom Air Force Base, Massachusetts, USA.
[3]Institute for Scientific Research, Boston College, Chestnut Hill, Massachusetts, USA.
[4]Institute of Space Science, National Central University, Chung-Li, Taiwan.
[5]Center for Space Physics, Boston University, Boston, Massachusetts, USA.

Paper number 2001JA001116.
0148-0227/01/2001JA001116$09.00

25 nT. This IMC was able to drive a major magnetic storm with minimum *Dst* of −167 nT at ~2400 UT on September 22. The most likely solar source was a faint but complete halo coronal mass ejection (CME) event seen at 0606 UT on September 20 which had a travel time of 63 hours (or a speed of 660 km s^{-1}) to reach Earth. The following month a CME recurrent with the September 20 event was observed at 0006 UT on October 18. This resulted in another major magnetic storm with minimum *Dst* of −231 nT, which occurred at 0700 UT on October 22, 1999. This latter CME was a partial 210° wide halo type which took 77 hours (or a speed of 540 km s^{-1}) to reach Earth. This storm has also been made part of the ISWP study. We will utilize both storms in this paper, to emphasize that ionospheric effects on specific communication or navigation systems are greatly dependent on the local time of maximum magnetic perturbations and not just on the magnitude of the perturbations. Thus we shall show that the September 1999 storm had a more severe effect on such systems in the United States than the October 1999 storm even though the latter was classified as a much bigger magnetic storm.

Since one of the major objectives of this enterprise was to provide as complete as possible space-based and ground-based observations of these space weather events, we tried to use several global databases to follow the effects of these storms on the total electron content (TEC) and plasma density irregularity structure of the middle- and low-latitude ionosphere. In particular, we chose to cover the middle-latitude ionosphere as an important Global Positioning System (GPS)-based navigation system is being developed for this region in the continental United States. Earlier morphological studies by *Aarons et al.* [1972] and *Aarons and Allen* [1971] have shown that the middle-latitude ionosphere is quite benign, its characteristics being generally determined by the diurnal, seasonal, and solar cycle variations in solar production. It is only during major magnetic storms that this predictable variability can be dramatically overturned as the high-latitude convection pattern expands equatorward. Numerous studies made over the last three decades using the Millstone Hill incoherent scatter radar and the TEC and scintillation network of the Air Force Research Laboratory have delineated the major features of ionospheric storms which result from large energy inputs to the upper atmosphere associated with major magnetic storms. *Foster* [1993] presents a good review of the results obtained starting from 1970. For instance, the enhancement of TEC during local dusk at 1800 LT is well known [*Mendillo et al.*, 1970]. *Rishbeth and Hanson* [1974] suggested that this increase was caused by advection of relatively dense plasma into the observing volume, a fact that was confirmed by observations made at Millstone Hill [*Evans*, 1973; *Buonsanto et al.*, 1979]. *Buonsanto* [1999] in his comprehensive review on ionospheric storms points out that this dusk effect of TEC increase should be distinguished from a more long-lived positive storm effect which is due to large-scale changes in the thermospheric circulation caused by heating in the auroral zone. After the TEC increase at dusk, particularly at high midlatitudes, there is a sharp transition to a negative phase, which can generally be attributed to the equatorward motion of the midlatitude trough [*Mendillo and Klobuchar*, 1975; *Buonsanto et al.*, 1979]. Geostationary satellite observations at 137 MHz made from Hanscom Field, Massachusetts, for which the subionospheric (350 km) location is $L = 2.8$ showed abrupt onset of scintillations during such major magnetic storms which were coincident with sharp TEC decreases and the appearance of stable auroral red (SAR) arcs [*Basu*, 1974]. At that time, Basu hypothesized that perhaps the same processes that give rise to SAR arcs at the equatorward edge of the plasmapause are also responsible for generating field-aligned plasma density irregularities of approximately kilometers to hundreds of meters scales that give rise to VHF scintillations.

In the intervening two decades many studies have provided evidence for the presence of intense convection electric fields in the expanded auroral oval [*Foster and Aarons*, 1988; *Yeh et al.*, 1991, and references therein] while transient fields penetrate equatorward of the shielding region at midlatitudes [*Gonzales et al.*, 1983; *Burke et al.*, 1998]. *Foster and Rich* [1998] provide a good summary of such results. Unfortunately, the Millstone Hill incoherent scatter radar (ISR) was not operating during these particular September and October storms, the ISR World Days being scheduled near the middle of the month in both cases. Thus, for these two storms we utilize the scintillation data from Hanscom Air Force Base (AFB), Massachusetts, the Digisonde data from Millstone Hill, and the TEC fluctuation data from the nearby station in Westford, Massachusetts, to monitor the small (approximately kilometers to hundreds of meters) and large (approximately tens of kilometers) scale irregularity behavior in conjunction with Defense Meteorological Satellite Program (DMSP) F12, F13, and F14 overflights to monitor the particles and fields and thermal density structure in the topside ionosphere. In addition, we utilize GPS TEC data from a latitudinal chain of International GPS Service for Geodynamics (IGS) stations to monitor TEC across the continental United States.

Since a major objective of the ISWP is to monitor the effects on technological systems, we chose to study the possible impact of these storms on the Wide Area Augmentation System (WAAS) of the Federal Aviation Administration (FAA). The WAAS is a system which provides corrections to enable aviation users of the Standard Positioning Service (SPS) GPS capabilities to achieve accuracy, integrity, and availability in all phases of flight from enroute through precision approach to airports [*Dehel et al.*, 1999]. One of the corrections provided by the WAAS to enable accuracy improvements is the correction for the signal delay due to the ionosphere. Users of the SPS GPS system are currently limited to the L_1 frequency (1.575 GHz) and are not directly able to measure the delay of the signal due to the ionosphere. The WAAS provides this delay information in the form of a grid of data, which is transmitted to the user as part of the corrections. One of the questions confronting the users of the WAAS system is the effect of ionospheric storms, with its associated steep TEC gradients particularly during the current sunspot maximum phase. It is thus important to establish their effects on system operation and to explore the possibility of impact mitigation through predictions.

While studying the midlatitude impacts, it became apparent that penetration electric fields during magnetic storms would also affect WAAS-like systems currently under development in countries such as Japan, India, and the Latin American region. We thus utilized a latitudinal chain of TEC stations operating from Bogota, Colombia, to Santiago, Chile [*Valladares et al.*, 2001], in conjunction with TEC fluctuation data at numerous low-latitude stations from the IGS network to provide a global description of such perturbations. The effect of amplitude scintillation on the GPS and VHF/UHF communication systems was studied by utilizing the Air Force Research Laboratory (AFRL) scintillation network in the South American and

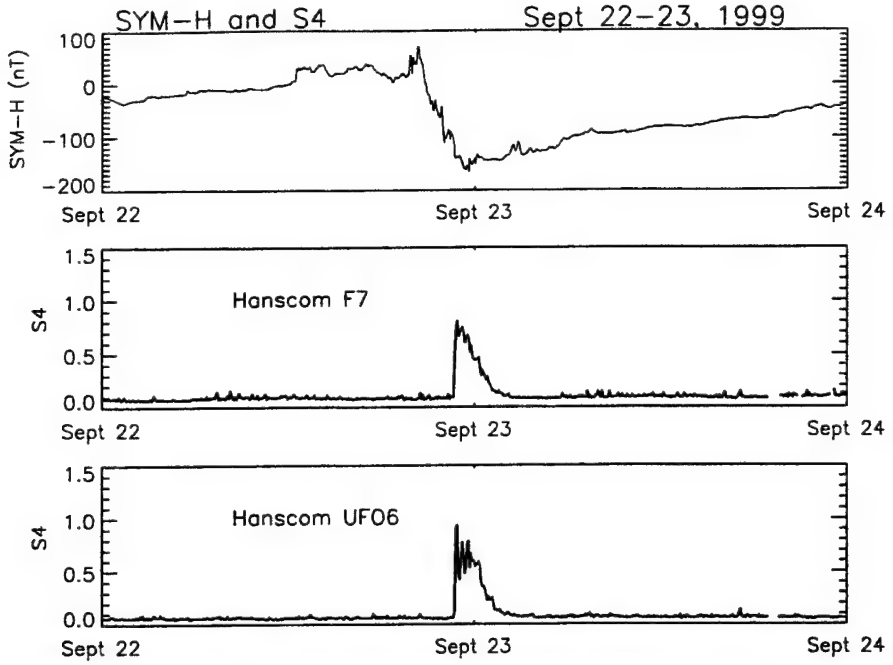

Figure 1. Scintillation index S4 at 250 MHz from two geostationary satellites Fleetsat 7 (F7) and UFO6 (U6) received at Hanscom Air Force Base (AFB), Massachusetts, plotted against SYM-H index for September 22–24, 1999.

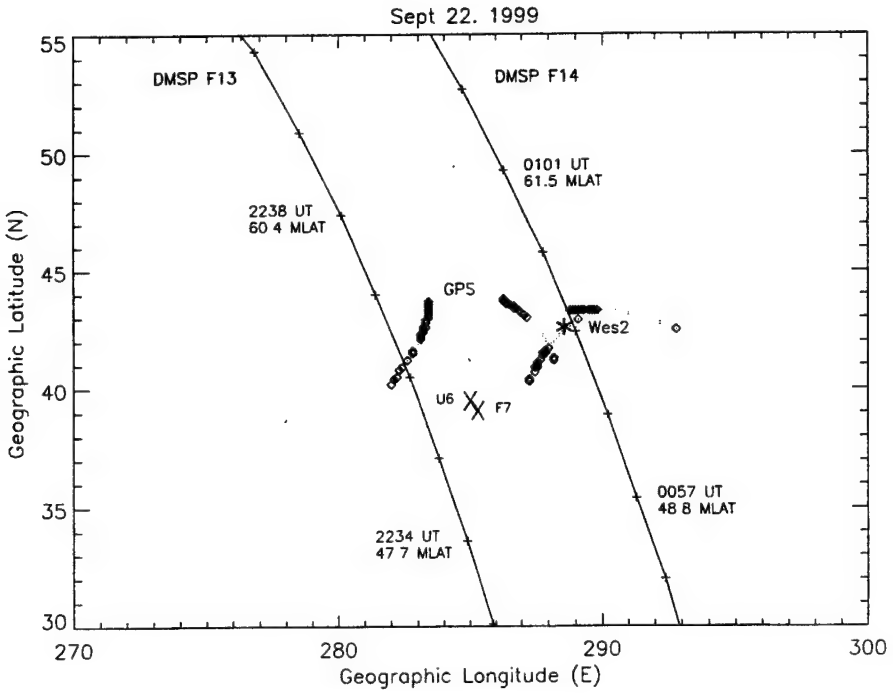

Figure 2. The 350-km intersection points for F7 and U6 for scintillation data from Hanscom AFB, Massachusetts, shown in Figure 1. Several subionospheric (350 km) tracks of GPS satellites from Westford (Wes2 indicated by a star) obtained between 2200 and 2400 UT on September 22 are also shown. The diamonds on the tracks indicate total electron content (TEC) fluctuations >1 TEC U min^{-1}. Two Defense Meteorological Satellite Program (DMSP) subsatellite tracks (indicated by solid lines) close to Hanscom are also shown; the F13 track is for 2233–2240 UT on September 22, and the F14 track is for 0056–0102 UT on September 23. The corrected magnetic latitudes (MLATs) of the 110-km field line mapped positions of the DMSP satellites are indicated along the tracks at two specific UTs.

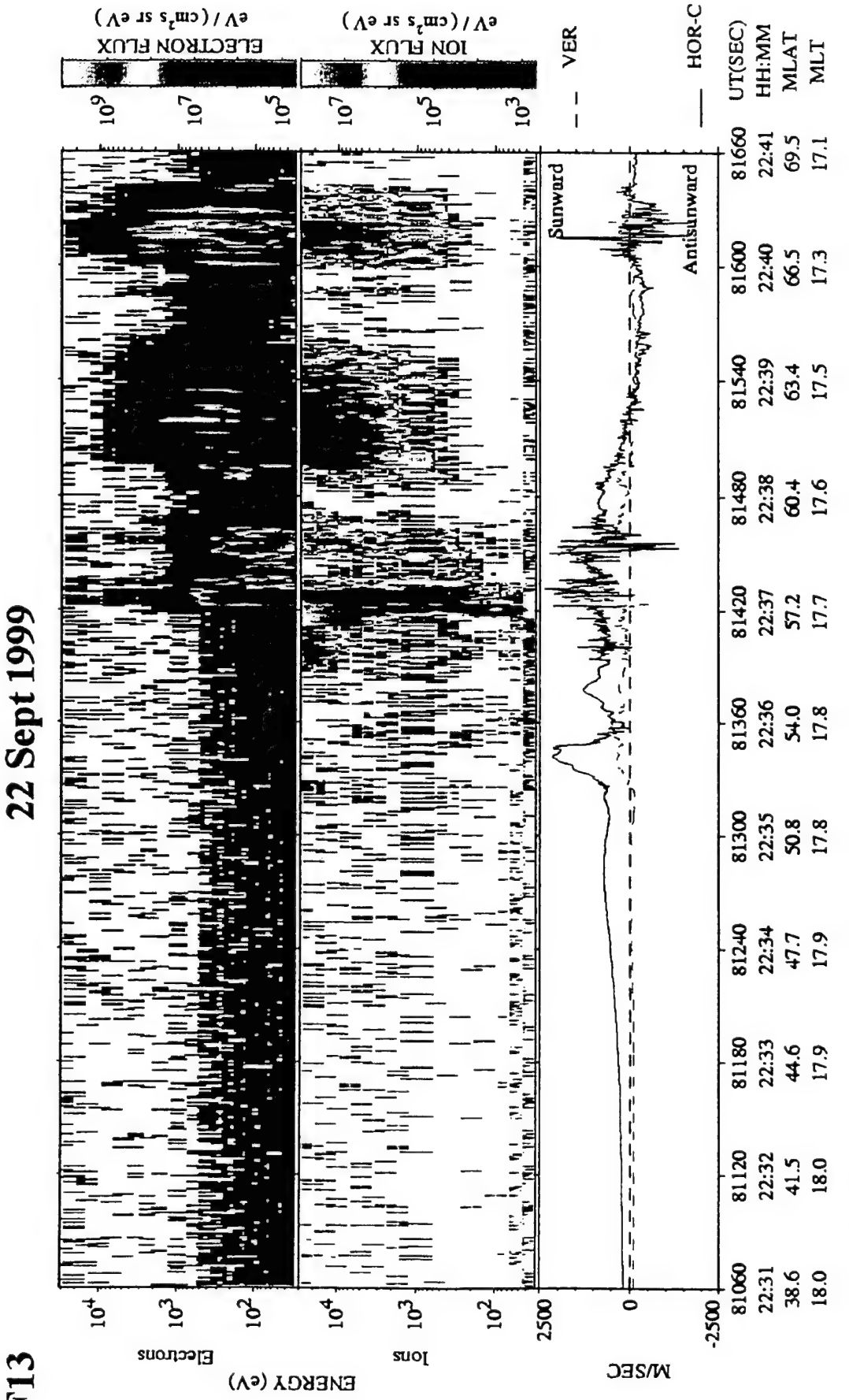

Plate 1. DMSP F13 measurements for the satellite track shown in Figure 2. The top and middle plots contain energy versus time spectrograms for downcoming electron and ion fluxes. Color codes for directional differential fluxes, particles (cm^2 s sr eV)$^{-1}$ are given to the right of the spectrograms. All parameters are plotted as functions of UT, MLAT, and the magnetic local time. The bottom plot gives the horizontal (solid line) and vertical (dashed line) components of plasma drift. A large horizontal and sunward drift structure of 2000 m s^{-1} is seen between 2235:20 and 2236:00 UT.

South Atlantic sectors. A novel feature is the extensive LT coverage provided by the high-resolution (1024 Hz) in situ measurements at 600 km from the Republic of China Satellite–1 (ROCSAT-1) with an inclination of 35° in addition to the coverage at 840 km provided by the Sun-synchronous DMSP satellites at specific LT.

2. September 22–24, 1999, Magnetic Storm

We will first present the perturbations in the middle-latitude ionosphere as a result of this magnetic storm and eventually follow the perturbations all the way to the equatorial ionosphere. Along the way, we will point out the possible impacts on WAAS and similar systems that may be operating under similar storm conditions.

2.1. Midlatitude Effects

The top panel of Figure 1 shows the high-resolution (1-min) values of the SYM-H index [*Iyemori et al.*, 2000], which closely follows the hourly *Dst* index developed by *Sugiura and Poros* [1971]. During this storm a fairly strong ring current developed with the SYM-H index reaching below −160 nT just prior to 2400 UT on September 22. The middle and bottom panels show the scintillation index S4 (defined by *Briggs and Parkin* [1963]) at 250 MHz from two geostationary satellites F7 and UFO6 plotted as a function of UT from Hanscom AFB, Massachusetts. The sudden onset of scintillations at 2240 UT on both ray paths as SYM-H (*Dst*) index drops precipitously is very evident. The geographic coordinates of the subionosphere (350 km) intersection are shown in Figure 2. The intersection points in the ionosphere are extremely close for the two geostationary satellites giving rise to simultaneous onsets of the scintillations. The orbits of two DMSP satellites and the subionospheric intersections of several GPS satellites obtained between 2200 and 2400 UT from the nearby station of Westford, Massachusetts, are also shown for subsequent use.

Earlier measurements by *Wygant et al.* [1998] on the CRRES spacecraft during the March 24, 1991, geomagnetic storm had shown that the large-scale magnetospheric electric field repeatedly penetrated into the inner magnetosphere between $L = 2$ and $L = 4$ when the rate of change of *Dst* was of the order of -50 nT h^{-1}. In this instance that rate of change was -75 nT h^{-1} between 2200 and 2300 UT on September 22, 1999. Thus the impulsive onset of scintillations at $L = 2.8$ (53° magnetic latitude (MLAT) in this longitude sector) for the Hanscom intersection points is in all likelihood linked to the appearance of electric fields and plasma density gradients in that vicinity. (For a discussion of the relationship between different magnetic coordinate systems in this longitude sector and the representation of DMSP positions in geographic and magnetic coordinates to be discussed below, see *Basu et al.* [1983a].) The scintillation event lasts for ~2 hours. The Millstone Hill radar has documented many instances of such fields and gradients at ionospheric heights [*Yeh et al.*, 1991; *Foster*, 1993; *Foster and Rich*, 1998]. Unfortunately, as mentioned earlier, the radar was not operating on that day, but the two DMSP orbits shown in Figure 2, particularly the F13, provides unmistakable evidence for a large penetration electric field in the vicinity of Hanscom at 1748 MLT, i.e., at dusk. Plate 1 shows DMSP F13 measurements taken at northern high latitudes on September 22, 1999, just west of the ionospheric intersection points for the F7 and UFO6 satellites in the early evening magnetic local time (MLT) sector between 2231 and 2241 UT. The top and middle plots contain directional differential fluxes of downcoming electrons and ions with energies between 30 eV and 30 keV in energy versus time color spectrogram format [*Hardy et al.*, 1984]. The bottom panel shows the horizontal and vertical components of the plasma drift obtained from the ion drift meter (IDM) on board the satellite [*Rich and Hairston*, 1994]. The most important point for our purpose is the large horizontal sunward drift of ~2000 m s^{-1} and a small generally upward drift seen between 52°–54° MLAT (2235:20–2236 UT) and straddling the two satellite intersection points equatorward of the energetic electron and ion precipitation boundaries. The sunward or westward drift is caused by a northward electric field of magnitude ~100 mV m^{-1} consistent with measurements at the Millstone Hill radar under similar conditions quoted above. Such westward and small upward drifts were also evident in the DMSP F14 data, the orbital track for which was shown in Figure 2.

Two other measurements, namely, those using the GPS receivers [*Doherty et al.*, 1994] and the Digisonde [*Reinisch and Xueqin*, 1983] provide evidence for an abrupt *F* region height rise and increase in the TEC. The TEC data from Westford, Massachusetts (42.6°N, 288.5°E), are shown in Figure 3 for September 22, 1999. These data are obtained by using the carrier phase and group delay measurements of GPS signals at L_1 (1.575 GHz) and L_2 (1.227 GHz) reported at 30-s intervals along the slant path from the receiver to the satellites. Using the ionospheric zenith angles, we convert the slant TEC to equivalent vertical TEC shown. The plot is obtained by combining TEC observations from the entire constellation of GPS satellites above 30° elevation over the 24-hour UT period and taking care of satellite and receiver biases in an appropriate manner [*Doherty et al.*, 1994]. Although the TEC variation is not as smooth as that seen on quiet days (quiet day behavior is shown in Figure 5), the most significant aspects of the data are the increase in TEC of ~10 TEC units (10^{16} el m^{-2}) around 2130 UT followed after 2200 UT by the precipitous drop of 35 TEC units at the very fast rate of ~1 TEC unit min^{-1}. Similarly, the Digisonde data (not shown) operating at this station also exhibit a sudden increase in the height of the ionosphere starting after 2135 UT followed by a large decrease in the critical frequency f_oF_2 (consistent with the approach of a trough) from 9.5 MHz at 2135 UT to 4.5 MHz at 2250 UT, and the ionograms show evidence of spread *F* throughout this time period. This afternoon height rise and TEC increase in the storm initial phase have been widely reported in the literature. They are considered to be a combined effect of an eastward electric field in the presence of sunlight and advection of plasma from lower latitudes [*Foster*, 1993, and references therein].

The precipitous drop in f_oF_2 and TEC is accompanied by large fluctuations in TEC starting at 2210 UT as shown in Figure 4. This diagram was obtained by considering the differential carrier phase data alone along the line of sight over each 30-s interval [*Pi et al.*, 1997; *Basu et al.*, 1999; *Bhattacharyya et al.*, 2000]. Figure 4 shows that TEC fluctuations were very small throughout the day until 2200 UT. Shortly thereafter, very large fluctuations, some as large ±5 TEC units min^{-1}, are seen for several tens of minutes on almost all the satellite ray paths visible from Westford at that time. The subionospheric tracks for these satellites were shown in Figure 2. The small diamonds along the GPS satellite tracks show the locations for which the TEC fluctuations were greater than 1 TEC unit min^{-1}. Large-magnitude fluctuations on the order of ±5 TEC

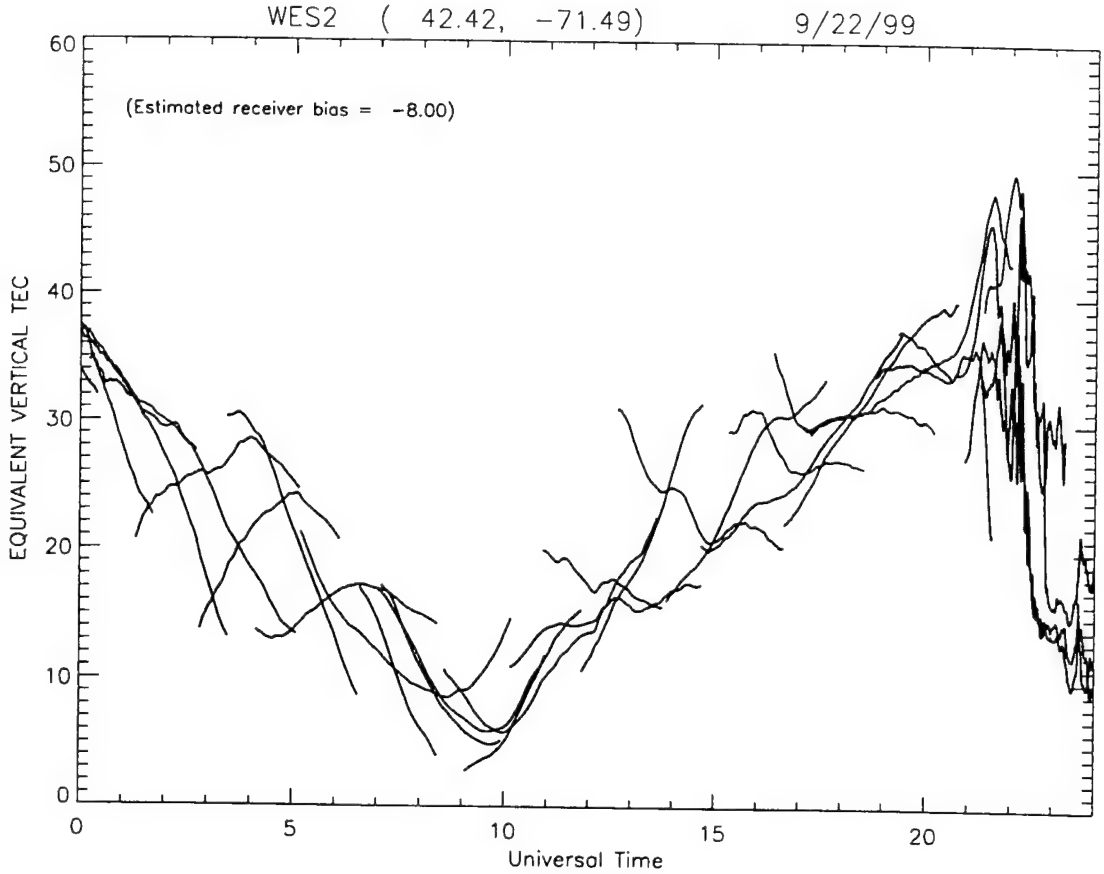

Figure 3. The equivalent vertical TEC measured using GPS satellites at Westford, Massachusetts (WES2), on September 22, 1999.

units min^{-1} are expected to be a problem for the WAAS system (A. J. Mannucci, private communication, 2000). If we consider the TEC fluctuations at Westford and the scintillations at Hanscom AFB to be two different manifestations of the irregular structure of the ionosphere, then it is possible to estimate the rate of equatorward motion of this irregularity front by considering the subionospheric separation between the TEC and scintillation ray paths and the delay in onset times. Using this separation to be 425 km and the delay to be 30 min, we obtain an average equatorward motion of ~230 m s^{-1} for the disturbance. Thus the 30-s sampling interval of the TEC fluctuations corresponds to a spatial scale of ~7 km or minimum resolvable north-south irregularity wavelengths of 14 km. In other words, the TEC fluctuations are caused by tens of kilometers scales as compared to the intensity scintillations at 250 MHz, which are caused by irregularities on the order of a kilometer or smaller (determined by the Fresnel dimension). Possible causes of these large- and small-scale irregularities will be discussed in section 4.

To determine the behavior of this large-scale gradient across the continental United States, where the WAAS system is to operate, we investigated the TEC behavior at the NE-SW chain of stations of the IGS network. The GPS TEC data from Westford, Massachusetts (WES2), North Liberty, Iowa (NLIB), Colorado Springs, Colorado (AMC2), and Pietown, New Mexico (PIE1), over a 4-day period covering the storm are shown in Figure 5. Their locations together with those of other IGS sites including stations in the equatorial region are shown in Figure 6. This diagram was kindly provided by X. Pi and shows a small subset of the total number of IGS stations [*Pi et al.*, 1997]. The TEC scale in Figure 5 is shown in terms of range delay to make this diagram more useful to the WAAS users. To compare Figures 3 and 5 one should recall that 6.15 TEC units is equivalent to 1 m of range delay at the GPS L_1 (1.575 GHz) frequency. The storm time TEC increase causes a range delay of 8 m at Westford rising to 12 m at lower latitudes. This is followed by a much more dramatic TEC decrease from 12 to 2 TEC units in the course of an hour at some stations, owing to the equatorward motion of the midlatitude trough. The motion of these large-scale features from N-S across the United States is very evident. An unexpected and sharp range delay change of this magnitude is expected to be of concern to WAAS users. The TEC behavior on September 21 is introduced as the normal quiet day behavior for comparison to the storm time behavior on September 22. While at Westford the storm time TEC curve shows mostly a change of shape (an abrupt increase followed by a fast decrease) with both the quiet day and storm TEC causing 6–8 m range delay, the TEC behavior at lower latitudes shows an increase from 8 to 12 m in the delay introduced by the ionosphere.

The TEC increase is followed by a severe decrease on September 23, first in the existence of very low nighttime TEC values in the trough followed by a significant decrease in TEC during the daytime. This is the well-known storm negative phase caused by a composition change of the ambient ionosphere [cf. *Buonsanto*, 1999, and references therein]. From the point of view of the WAAS users, a decrease of 4 m in the range delay is expected at most stations during the daytime due to the storm negative phase.

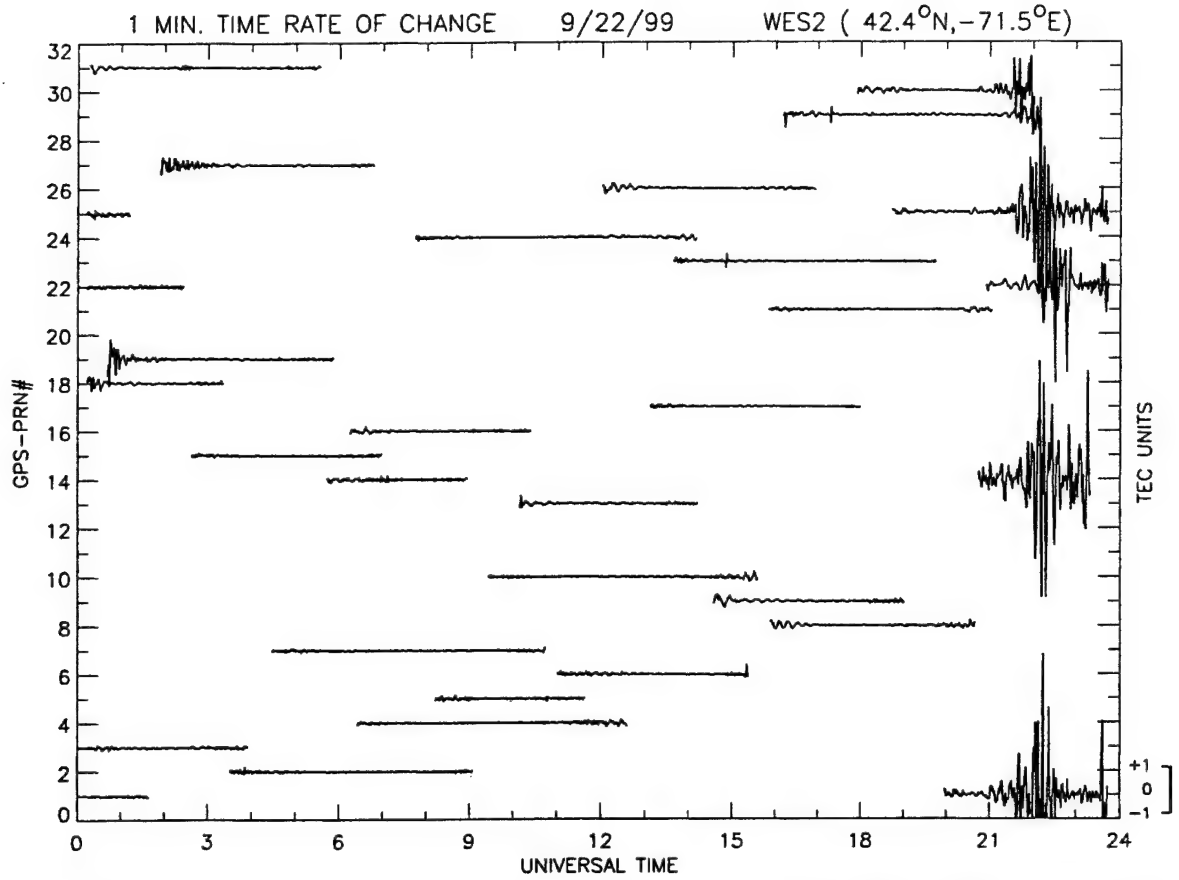

Figure 4. The time rate of change of TEC in TEC units (10^{16} el m^{-2}) min^{-1} measured using data shown in Figure 3 at Westford, Massachusetts (WES2), on September 22, 1999.

However, since this is a gradual change, it is much easier to accommodate than the TEC increase and decrease at the storm onset. Normal TEC values giving rise to expected range delays are finally approached on September 24. Thus the ionospheric storm caused as a result of the magnetic storm has a large measurable impact on a navigation system operating in what was expected to be a relatively benign midlatitude ionosphere.

2.2. Equatorial Effects

The effect of the magnetic storm seemed to create enhanced effects at lower mid-latitudes as evidenced by the TEC behavior shown in Figure 5. This was interpreted as a combined effect of the prompt penetration of the eastward electric field into the ionosphere and the storm-enhanced plasma density and consequent TEC increase seen in the dusk sector by *Foster* [1993]. A natural extension of this midlatitude study seemed to be the investigation of the effect of this prompt penetration on equatorial scintillations and TEC gradients and their consequent impacts on WAAS-like systems being developed for low latitudes.

An important feature of the low-latitude *F* region is the presence of the equatorial anomaly, with peaks in the plasma density at ±15° dip latitude and minima at the magnetic equator. They are the result of the upward motion of the plasma at the magnetic equator and its consequent diffusion along the magnetic field lines [*Hanson and Moffett*, 1966]. The TEC anomaly starts to develop as early as 1100 LT. The crests move away from the equator with increasing local time, as the *F* region at the equator moves to higher altitudes and reaches a maximum development around the afternoon hours [*Basu and Das Gupta*, 1968]. On some evenings a strong resurgence of the anomaly takes place; this is probably due to the well-known prereversal enhancement (PRE) of the vertical drift, which generally occurs around 1900 LT [*Woodman*, 1970; *Tanaka*, 1981]. A well-developed PRE has been found to be one of the most important indicators associated with the onset of equatorial spread *F* (ESF) by *Basu et al.* [1996] and *Fejer et al.* [1999]. In a very recent paper, *Valladares et al.* [2001] have shown the existence of a close relationship between the temporal evolution of the TEC profiles as a function of latitude near sunset and the onset of ESF. Their data came from the year 1998. We utilize that array of TEC stations in South America extending from Bogota, Colombia, to Santiago, Chile, in conjunction with ground scintillation observations from Ancon, Peru, and Antofagasta, Chile, shown in Figure 7, to study the effect of this magnetic storm on the equatorial ionosphere.

The scintillation data from Ancon, Peru, using the F8 satellite are shown in Figure 8. It starts rather abruptly at 2308 UT (1808 LT), as is generally the case at equatorial stations [*Basu et al.*, 1978]. However, there are two surprising aspects to these measurements. One is the start of the scintillations at 1808 LT, which is actually 15 min before *E* region (100 km) sunset at the satellite intersection point, and the other is the total absence of scintillations throughout the night at the F7 intersection point to the west of Ancon, which is separated from the F8 intersection point by 630 km. Thus it seems that the scintillation onset

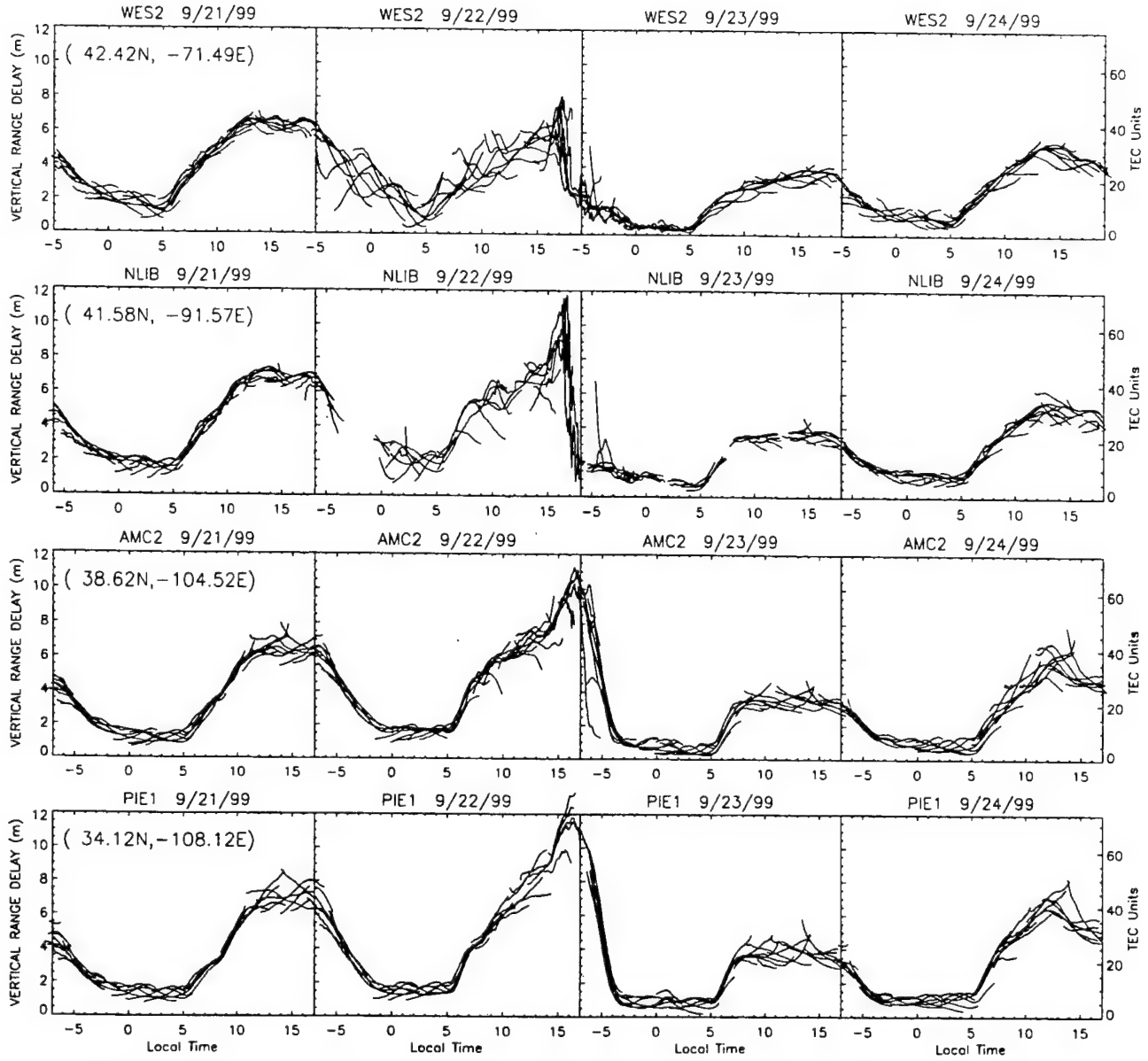

Figure 5. Range delays recorded at four stations in the International GPS Service for Geodynamics (IGS) network, namely, Westford, Massachusetts (WES2), North Liberty, Iowa (NLIB), Colorado Springs, Colorado (AMC2), and Pietown, New Mexico (PIE1), during September 21–24, 1999. Range delay can be related to TEC at 1.575 GHz by noting that a 6.15 TEC units change causes a 1-m range delay.

is related to the prompt penetration of eastward electric field made possible by the conductivity gradients near sunset. Further, the equatorial prompt penetration at dusk was very localized in longitude. There was no scintillation at 1.7 GHz for the Antofagasta G8 ray path which was within the irregularity zone, thereby indicating that the integrated strength of turbulence caused by the disturbance was not large enough to create perturbations at such a high frequency. The scintillations on both F7 and F8 ray paths during the evening of September 21–22 from Ancon are most likely due to the expected occurrence of ESF on normal quiet days at equinox during solar maximum in the Peruvian sector [*Aarons*, 1993].

In the absence of Jicamarca radar data we utilized the array of GPS TEC stations shown in Figure 7 to study the latitudinal behavior of TEC in the hope of getting some clues to the vertical plasma drift behavior which may have some bearing on the scintillation asymmetry to the west and east of Ancon. The latitude variation of TEC was computed by utilizing GPS data as was done by *Valladares et al.* [2001] the only difference being that the latitude variation was computed separately for data obtained to the west and east of 72°W longitude. Further, only the data from the southern half were utilized, because of the gaps in the chain to the north. Our scintillation ray paths also intersect close to the magnetic equator and to the south of it. The data in Figure 9 show a fairly remarkable difference between the east and west cuts with the former showing evening anomaly peak development at 1800 UT (2300 UT) and 1900 LT (0000 UT) whereas the latter shows TEC peaks at the equator, thereby indicating that the evening anomaly had not formed in the west. While this does not provide a cause for the difference, this asymmetric behavior provides evidence for the enormous importance of the PRE of the vertical drift in the generation of ESF.

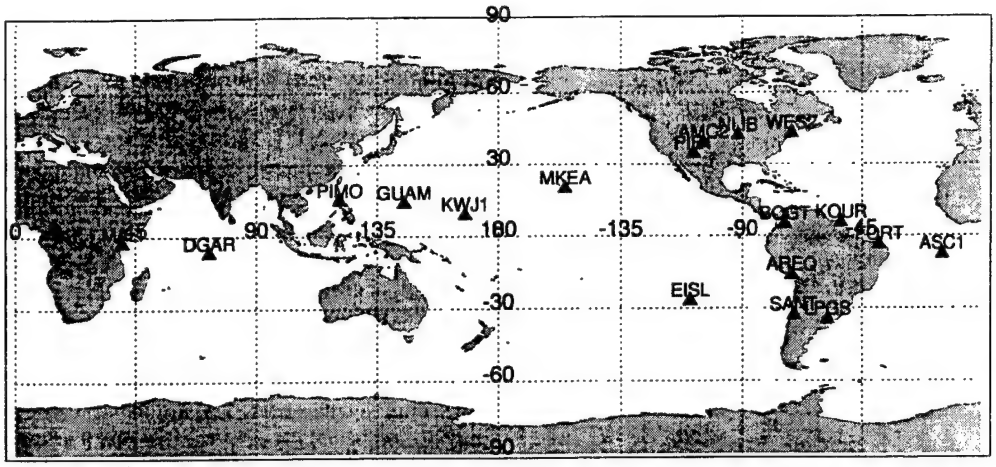

Figure 6. Global map showing IGS stations that provided data for this study. MALI, Malindi; DGAR, Diego Garcia; PIMO, Manila; KWJ1, Kwajalein; MKEA, Hawaii; EISL, Easter Island; BOGT, Bogota; KOUR, Kourou; AREQ, Arequipa; SANT, Santiago; LPGS, LaPlata; FORT, Fortaleza; ASC1, Ascension Island.

The TEC and scintillation data taken together provide indirect proof that the westward boundary of the penetration electric field in the equatorial region is probably close to 73°W (287°E). To provide an eastward boundary, we checked several global databases, both space- and ground-based. The DMSP F12 and F14 data of topside densities at 840 km, which crossed the magnetic equator at 321°E at 2318 UT and 324°E at 2306 UT, respectively (near the eastern edge of Brazil), were the only ones to show perturbations in the form of density depletions in the equatorial region. These passes are at 2100 LT, and one expects irregularities to show up in the topside by this time. No other passes in the vicinity showed any signatures of topside disturbances. Unfortunately, the ROCSAT-1 data were not available during the night of September 22–23. This is because the severe Taiwan earthquake of September 21 knocked out power to the mission operation centers for a couple of days.

In terms of ground-based data sources form the IGS network, the TEC fluctuation data of the type shown in Figure 4 for Westford were checked for many equatorial stations at different longitudes shown on the global map in Figure 6. There was an absence of fluctuations at Hawaii (MKEA), Easter Island (EISL), Bogota (BOGT), Arequipa (AREQ), and Santiago (SANT), i.e., stations on islands in the Pacific Ocean and along the west coast of South America. However, TEC fluctuations were observed at Kourou (KOUR), Fortaleza (FORT), and LaPlata (LPGS) on the east coast of South America. The TEC fluctuations started at 2110 UT in Fortaleza, Brazil (*E* region sunset is 2107 UT), and continued intermittently up to 0800 UT on September 23; the magnitude, however, never exceeded ±2 TEC units min^{-1}. The Fortaleza ground-based data are thus consistent with the DMSP F12 and F14 orbits presented earlier. Both scintillations and IGS data are available from Ascension Island (ASC1). The Ascension Island 250-MHz scintillation data had an abrupt onset at 2127 UT (2027 LT), i.e., a fairly late start for a station where *E* region sunset is at 1930 UT with no gigahertz scintillation observed that night. This probably indicates that the scintillation was caused by structures that drifted in from the west. The Ascension Island IGS data showed significant TEC fluctuations after 2100 UT and continued intermittently up to 0400 UT.

Unfortunately, no IGS stations are available on the west coast of Africa, the closest one being on the east coast at Malindi (MALI), which showed no storm-related TEC perturbations. For completeness, we checked the station at Diego Garcia (DGAR) and those in the Far East such as Manila (PIMO) and Kwajalein (KWJ1). However, since the time of storm onset corresponds to the postmidnight to morning hours at these stations, no perturbations in TEC were detected. No late time disturbances, such as that attributed to the prompt penetration due to a northward turning of the IMF (see the overshielding concept discussed by *Kelley* [1989]) or that due to the ionospheric disturbance dynamo [*Blanc and Richmond*, 1980; *Fejer et al.*, 1999], were detected on the western side of South America for this particular storm. However, the TEC fluctuation data for Fortaleza and the 250-MHz scintillation data from Ascension provide evidence for a postmidnight event in the 0300–0500 LT time frame. Using ACE data, we found that the northward turning of the IMF for this storm had taken place at 0048 UT, if the expected propagation delay is included (J. Fedder, private communication, 2001). This is pre-midnight LT for both Ascension Island and Fortaleza, such that the prompt penetration due to overshielding is not expected to lead to fresh irregularity generation. Thus it seems that the postmidnight event is probably due to the effect of the disturbance dynamo alone. Unfortunately, no postmidnight zonal drift data were available that could have put this hypothesis on a firmer footing.

Given the various caveats we have mentioned, this storm in its development phase seemed to have had a positive effect on irregularity formation rather than an inhibition on the generation of equatorial irregularities in a very limited range of longitudes between 73°W and 15°W. In other words, the prompt penetration of the electric field in the eastward direction due to increased magnetospheric convection seemed to be confined to the longitude region which was close to the *E* region sunset for the UT range over which SYM-H (*Dst*) showed maximum variation including the time period when it remained at its most minimum level. Any positive late time effect also seemed to be confined to a part of this longitude range. We will return to a discussion of this point vis-à-vis the findings of storm time electric field models [*Spiro et al.*, 1988;

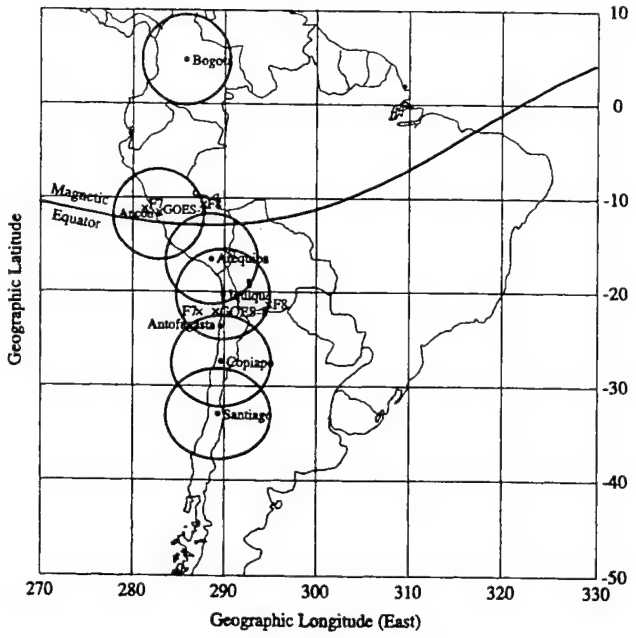

Figure 7. Equatorial array of GPS stations on the west coast of South America providing latitude variation of TEC data. The circles around the stations indicate 30° elevation coverage. Also shown are 350-km ionosphere intersection points to Fleetsat 7 (F7), Fleetsat 8 (F8), and GOES 8 from Ancon, Peru, and Antofagasta, Chile.

Fejer and Scherliess, 1997; *Scherliess and Fejer*, 1997] in section 4.

3. October 21–23, 1999, Magnetic Storm

We will follow the scenario used for the September 22–24 storm to describe this major October storm.

3.1. Midlatitude Effects

In Figure 10 we show the VHF scintillation data from two geostationary satellites observed at Hanscom AFB plotted against the high-resolution SYM-H index. The onset of scintillation at 0120 UT and 0440 UT on both ray paths is well correlated with the two times of fast reductions in the SYM-H (or *Dst* index) between 0000–0200 UT and 0400–0600 UT, each of ~45 nT h^{-1}. The minimum value of −230 nT for SYM-H was reached around 0700 UT on October 22. While the first scintillation region is ~100 min wide, the second interval of high scintillation is 4 hours long, which includes 2 hours of moderate scintillation.

In the absence of the Millstone ISR data, we utilize the Digisonde located there and are benefited by the 5-min sounding interval specially used for the ISWP as shown in Figure 11. The fall in f_oF_2, from a flat peak of 12 MHz starts from 2100 UT on October 21 (not shown) and is part of a gradual sunset decay. It is greatly accelerated beyond 0050 UT on October 22 when f_oF_2 falls from 7.5 to 3.1 MHz (a factor of almost 6 decrease in N m F_2) at 0235 UT with high values of hmF_2, the height of the peak of the F_2 layer (both characteristics of the trough). It is interesting to note that even though it is close to local midnight, f_oF_2 starts increasing to a value of ~6.0 MHz at 0545 UT (0045 LT), and an E region makes its appearance between 0400 and 0650 UT. Between 0650 and 0745 UT there is a gap in the data. These effects are generally thought to be due to a varying spectrum of particle-induced ionization. Soft particles can cause F region ionization, with some E region contribution, and then with a hardening of the precipitating particles affecting the D region, we eventually reach a point at which the F region cannot be seen at all because of increased radio-wave absorption (J. W. Wright, private communication, 2001). During the entire time period between 0100 and 1100 UT (except the gap region mentioned above), the ionograms

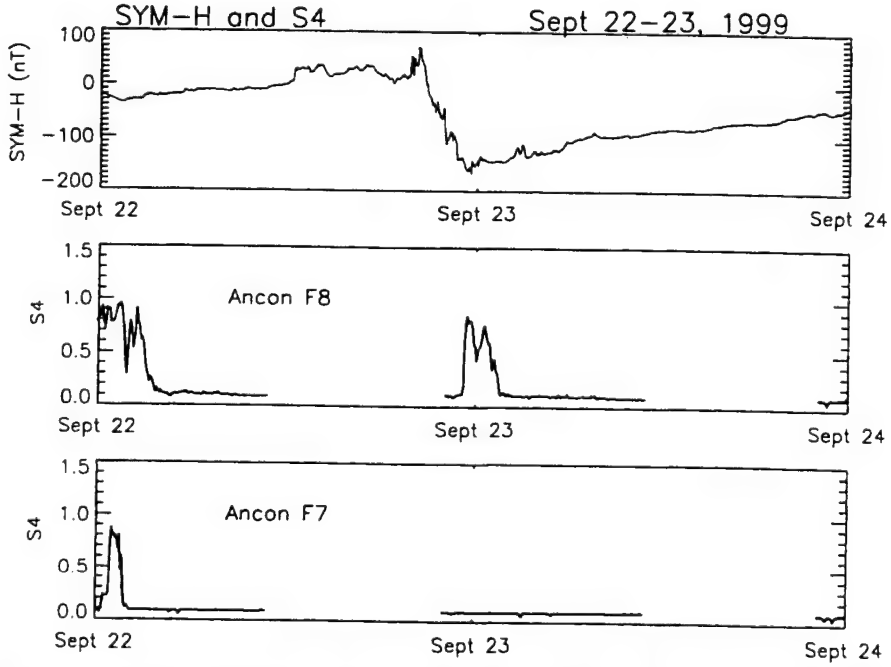

Figure 8. Scintillation at 250 MHz from two geostationary satellites Fleetsat 7 (F7) and Fleetsat 8 (F8) recorded at Ancon, Peru, plotted against the SYM-H index for September 22–24, 1999. Note the complete absence of scintillations on F7 during the evening of September 22–24, 1999. Note the complete absence of scintillations on F7 during the evening of September 22–23, 1999.

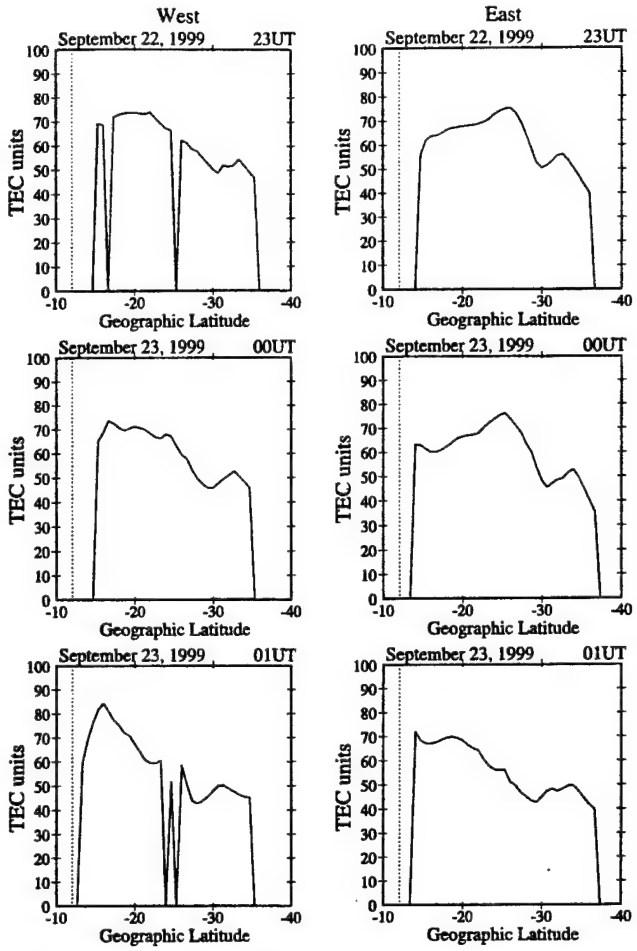

Figure 9. The latitude variation of TEC using the southern half (in magnetic latitudes) of the array computed to the west and east of longitude 72°W. While the data from the eastern half show a clear formation of the equatorial anomaly at 2300 UT (1800 LT) on September 22 and 0000 UT (1900 LT) on September 23 at 25°S (15° magnetic latitude), the western half does not show any evidence for anomaly development with the TEC peak being close to the magnetic equator. The abrupt discontinuities in the plots are the result of data dropouts.

show evidence of spread *F* with the magnitude of *df/f*, where *df* is the frequency spread around the critical frequency, being on the order of 10%.

The equivalent vertical TEC data for October 22, 1999, from Westford, Massachusetts, are shown in Figure 12 and are obtained exactly as detailed in the description for Figure 3. The quick fall in TEC beyond 0000 UT (1900 LT) to below 10 TEC units is very evident. Also very prominent is an increase in TEC to ~20 TEC units between 0400 and 0800 UT. This is followed by another decrease until sunrise the next morning at 1100 UT (0600 LT) when TEC gradually increases in value but reaches a maximum which is only half that seen on the previous day (compare Plate 2). This is quite consistent with the extended negative phase following major magnetic storms due to composition changes in the ionosphere [cf. *Buonsanto*, 1999].

The TEC fluctuations for October 22 on each GPS satellite are shown in Figure 13. Again, this is obtained in a manner similar to Figure 4. It is rather interesting to note that the TEC fluctuations in the vicinity of 0100 UT associated with the quick TEC fall brought about by the equatorward motion of the trough are rather moderate (±1–2 TEC units) compared to the September 22 case. The large TEC fluctuations in this case (some as large as ±4 TEC units) are primarily confined to the period between 0630 and 0800 UT, which covers the time when the Digisonde was unable to record the background ionospheric parameters due to increased absorption. It is rather important to note from Figure 12 that these large TEC fluctuations are confined to the trailing edge of the TEC enhancement near local midnight. Since *AE* (>1000 nT) and SYM-H or *Dst* (>−200 nT) were both at extreme levels at this time, and the ionograms showed evidence of auroral particle precipitation, it is a very reasonable assumption that this TEC increase is due to an auroral blob generated locally and/or convected into this region whose trailing edge has been structured by the gradient drift instability [*Basu et al.*, 1990]. We will return to a discussion of this point in section 4.

This October 1999 storm was very important from the point of view of the WAAS prototype testing. This was the first major magnetic storm, which could be used to observe the robustness and accuracy of early WAAS algorithms in operation. Plate 2 displays TEC from four stations in the IGS network going from NE to SW (clockwise starting from lower right), as was done in Figure 5 for the September 22 storm. In the October case, however, each station TEC (expressed in terms of vertical range delay) has a vertical range delay overplotted in red. These vertical range delays were obtained from the estimated ionospheric vertical delays provided by the WAAS Ionospheric Grid Points (IGPs). In the panels directly below the TEC data we show the WAAS parameter called Grid Ionospheric Vertical Error (GIVE). The GIVE values are the estimated errors in the IGP values. Plate 2 illustrates that GIVE values increased to 6 m or more when short-term fluctuations were seen in TEC between 0000 and 1000 UT on October 22 (1900 LT on October 21 to 0500 LT on October 22 for Westford). At other times, GIVE values rarely exceeded 1.5 m. As in the case of Figure 5, Plate 2 also shows larger storm effects at the lower-latitude stations in Colorado and New Mexico. In an operational WAAS an aircraft user will interpolate the grid of IGPs for a local vertical range delay, apply that vertical delay to all satellites in view, and then use the GIVE values as an input to a function which estimates overall position error [*Dehel et al.*, 1999]. The impact of ionospheric storm activity on WAAS is currently under intense investigation by a WAAS Ionospheric Working Group (WIWG) (P. Doherty, private communication, 2000). The results shown in Plate 2 are representative of early attempts to observe WAAS behavior during magnetic activity. In general, the September 1999 storm had a much larger effect on the midlatitude ionosphere in the continental United States as compared to the October storm, because the storm's main phase came at an earlier local time even though the October storm had a large negative SYM-H (*Dst*) per se.

3.2. Equatorial Effects

Following the same logic of studying the effect of the penetrating electric fields on the equatorial ionosphere as in section 2.2, we turn our attention to the equatorial region. The plasma density irregularities associated with this storm produced a widespread effect, in terms of longitude coverage, and long-lived effects, in terms of time coverage. The ROCSAT-1 measurements allowed us to track both these variabilities in a meaningful way. This satellite with the Ionospheric Plasma and Electrodynamics Instrument (IPEI) on board was launched on

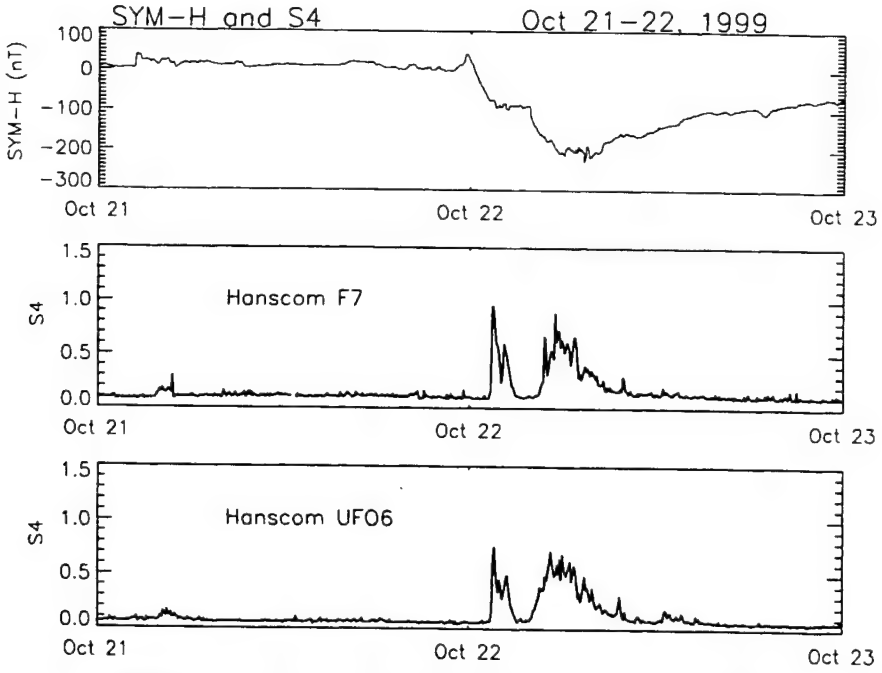

Figure 10. Same as in Figure 1 but for October 22–23, 1999.

January 27, 1999, into an almost circular orbit near 600 km with inclination of 35° [*Yeh et al.*, 1999]. Supporting information was obtained from DMSP F12, F13, and F14, the ground scintillation data, and the TEC data from the IGS network.

One of the more interesting aspects of the scintillation data for this storm is the nearly simultaneous onset at all three Ancon and Antofagasta (F7, F8, and G8) ray paths whose positions were shown in Figure 7. One set of such measurements for the Ancon F7 (at 250 MHz) and G8 (at L band) satellites is shown in Plate 3 for October 22 (Plates 3a and 3d) together with the spaced receiver drift measurements [*Basu et al.*, 1986; *Valladares et al.*, 1996] and power spectral densities (psds) at three specific irregularity scale lengths in Plates 3b and 3c (the drifts and psds are discussed later in the section). The scintillation, particularly at 250 MHz, continued for a long period of time. The simultaneous scintillation onset at these different ray paths and the persistence of scintillations for a long period through the night can be better understood by considering the coordinated density and velocity data from ROCSAT-1.

In Figure 14 we present the data from ROCSAT-1 which were taken at 1024 Hz (but plotted at 1 Hz) for the first two successive orbits on October 22. The data in the top panel shows a snapshot of a series of depletions in density, also known as plasma bubbles [*McClure et al.*, 1977], seen between 0011:30 and 0021:20 UT covering a longitude range within which most of the ray paths from Ancon and Antofagasta intersect except the western fringe (when presumably the satellite moved out of the equatorial irregularity belt). This orbit obtained immediately after storm onset (IMF B_z south) shows the presence of enhanced eastward electric field of 1–2 mV m^{-1} in the evening period compared to the quiet day pattern on October 20, 1999 (H.-C. Yeh, private communication, 2001). This indicates that the effect of the prompt penetration of the electric field has reached equatorial latitudes. The presence of plasma bubbles and scintillations associated with an eastward electric field indicates that the Rayleigh-Taylor instability mechanism is operative over a wide swath of longitudes [*Ossakow*, 1981].

The next ROCSAT orbit at 0145 UT (bottom panel of Figure 14) shows a further development of bubbles with a series of depletions extending from 267° to 300°E longitude straddling the magnetic equator with the deepest depletion containing only 10^2 cm^{-3} located close by. The velocity measurement for this orbit shows a continued presence of an enhanced eastward electric field in the evening period. What is more interesting is the gradual development from westward in orbit 1 to an eastward electric field in orbit 2 over the postmidnight time frame (H.-C. Yeh, private communication, 2001). The latter probably indicates a development of the disturbance dynamo after the storm has continued for a couple of hours. The highest density exceeding 10^6 cm^{-3} is seen at the northern crest of the equatorial anomaly in both the top and bottom panels that constitute orbits 1 and 2 for October 22. Presumably, ROCSAT was sampling the irregularities in the immediate topside, as the F peak tends to be high during sunspot maximum at equinox. It is the irregularities on the high-density walls of such depletions or bubbles that give rise to intense VHF and gigahertz scintillations [*Basu et al.*, 1983b]. It should be noted from the scintillation data on the top and bottom panels of Plate 3 that while the amplitude scintillation at VHF is intense (S4 $\sim$ 1) for several hours, the L band G8 scintillation is weak with S4 $<$ 0.2. On this night the simultaneous G8 data from Antofagasta (not shown) showed S4 $>$ 0.5 up to 0530 UT. It is the greater background density near anomaly peak stations that gives rise to the larger magnitude of scintillations even when bubble structures are seen throughout the equatorial belt. On this night, severe scintillations were observed particularly in a southerly direction, i.e., toward the southern anomaly crest on the GPS $L1$ frequency at Antofagasta with the scintillation maximizing at S4 of 1.2 between 0100 and 0200 UT as shown in Figure 15. Such high levels of S4 on so many different ray paths may pose a problem for WAAS-like systems in the equatorial region.

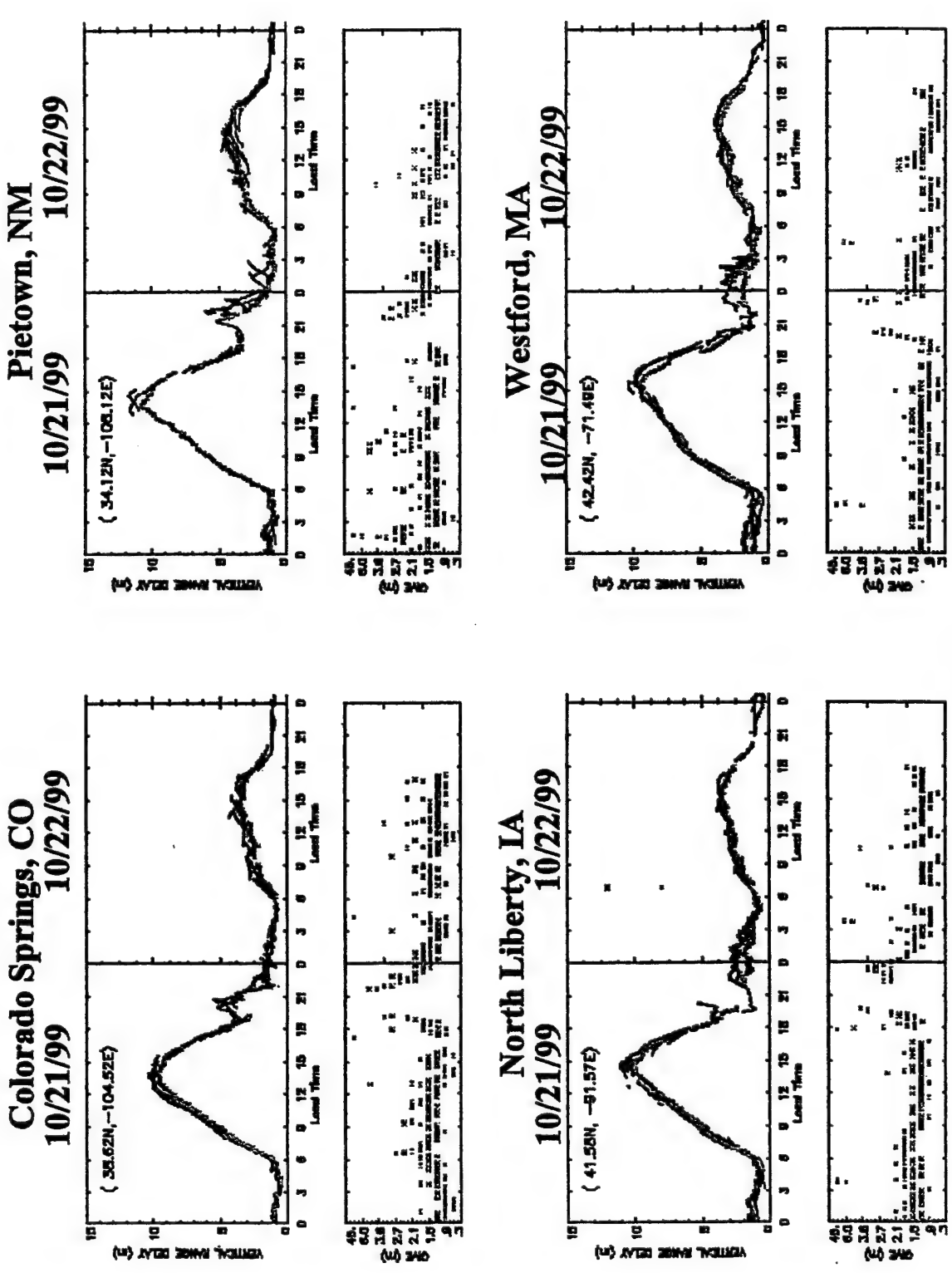

Plate 2. Similar to Figure 5 but for October 21–22, 1999, which has an estimated Wide Area Augmentation System (WAAS) range delay overplotted in red. The output of the WAAS error-bound algorithm called Grid Ionospheric Vertical Error (GIVE) is plotted in meters (m) on the lower panel, and also in red, for each station.

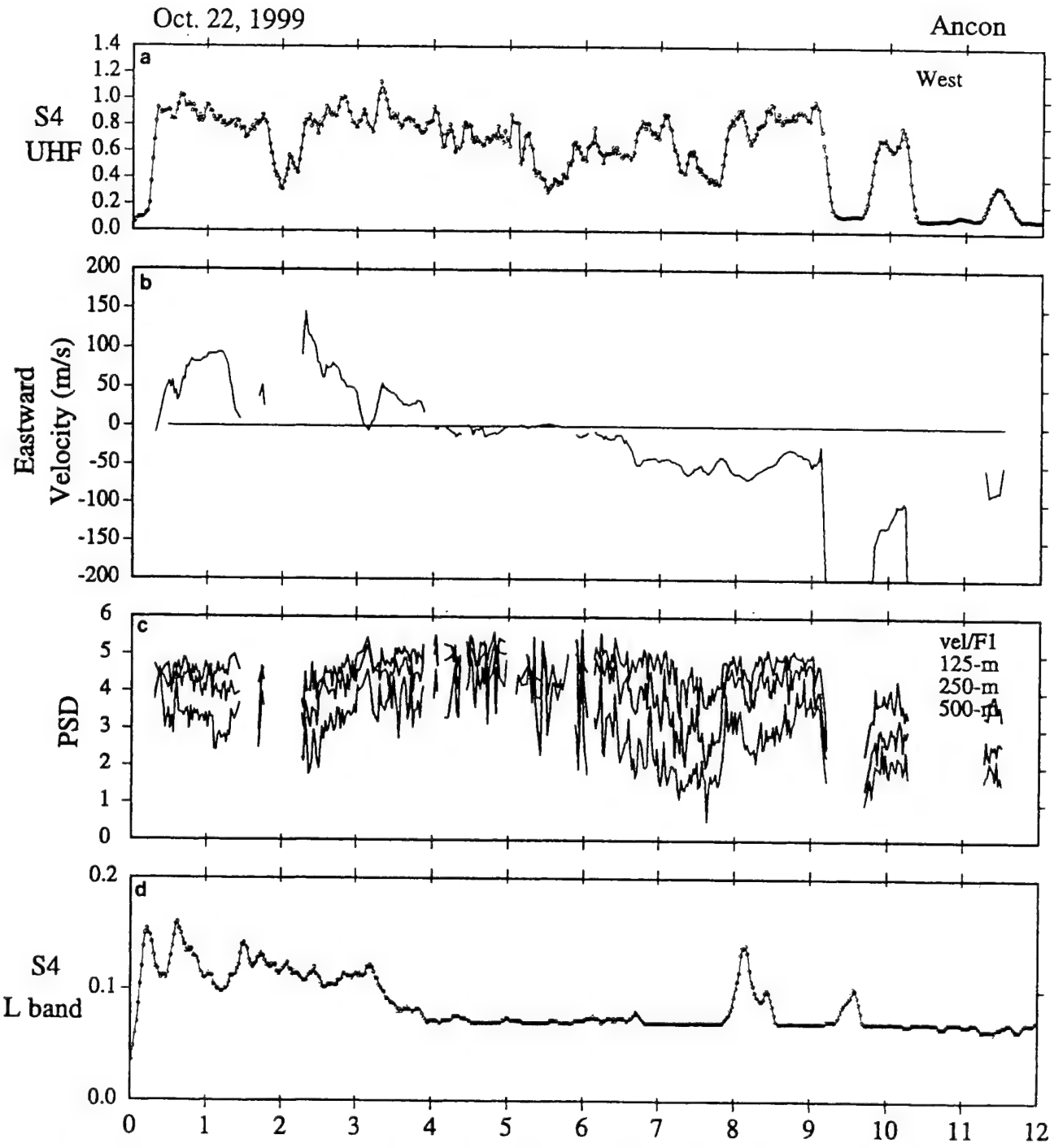

Plate 3. Scintillation data obtained at Ancon, Peru, on October 22, 1999. (a) The 250-MHz (UHF) data from F7 (to the west). (b) The E-W irregularity drift from spaced receiver measurements using the F7 satellite. (c) Power spectral densities in dB Hz^{-1} at 500, 250, and 125 m on a logarithmic scale obtained by combining the fast Fourier transform spectra and the E-W irregularity drift shown in Plate 3b. (d) The 1694-MHz (*L* band) data from G8.

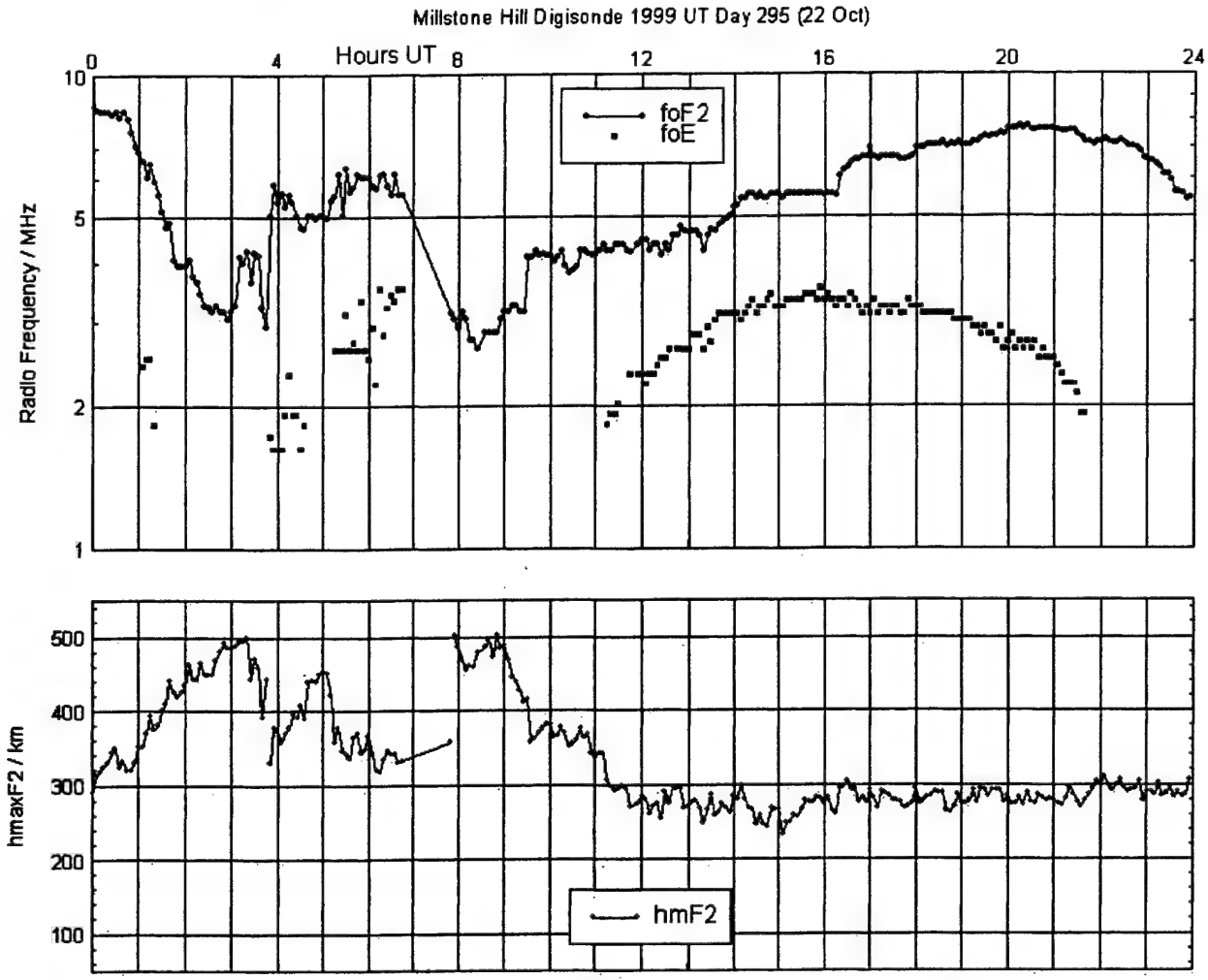

Figure 11. Digisonde data showing the F layer critical frequency f_oF_2, the E layer critical frequency f_oE, and the maximum height of the F layer hmF_2 observed at Westford, Massachusetts, on October 22, 1999. Note that the appearance of f_oE between 0400 and 0700 UT (2300–0200 LT) implies the presence of auroral particle precipitation. The break in the data from 0700 to 0800 UT is caused by increased absorption.

While the ROCSAT-1 gives a good idea of the E-W extent of the irregularities in the early evening hours, the DMSP F12 and F14 satellites provide a N-S cut through the equatorial irregularities that percolate to the topside and moreover provide a good coverage through the middle latitudes as well. Figure 16 shows the density at 840 km observed by F14 with an equatorial crossing near 0120 UT and one from F12 at 0140 UT both providing an approximate N-S cut through ROCSAT orbit 2 between 0155 and 0200 UT. Both the F14 and F12 orbits provide evidence for a wide belt of equatorial irregularities covering ±20° of magnetic latitude. They also provide evidence for deep depletions (10^3 cm^{-3}) reaching the topside. Within the depletions the drifts (not shown) are upward and westward with the background vertical and horizontal drifts being quite small.

In addition to the equatorial density (there is a break in the data for F14) the midlatitude density behavior seen in both DMSP orbits is very consistent with the Digisonde and TEC data from Westford presented in section 3.1. Both types of data show a deep trough at 52° magnetic latitude followed by a density increase or blob poleward of the trough. The DMSP orbits pass just to the west of the Westford (W) station as shown in the top panel of Figure 16. It is quite conceivable that the auroral blob may be convected equatorward to ~50°N magnetic latitude at later UT as a result of the continued intensification of the magnetic storm up to 0700 UT. As a matter of fact, the DMSP orbits show that there is very little of the entire nighttime global topside ionosphere that is not disturbed.

To return to the equatorial ionosphere, we consider the zonal irregularity drifts shown in Plate 3b. The drifts are mostly eastward in the range of 50–100 m s^{-1} between 0100 and 0300 UT and then decrease gradually to very small values between 0400 and 0600 UT, turn actually westward at 0630 UT, and continue in that direction with a magnitude of 50 m s^{-1} (with some larger values) until ~1200 UT (0700 LT) when the data ends. (There was a small-magnitude scintillation event between 1300 and 1400 UT that is not shown.) Drifts usually turn westward at sunrise [*Woodman*, 1972]. Thus the reversal past local midnight during this magnetically disturbed period is, in general, considered to be the effects of an ionospheric disturbance dynamo setting up a neutral wind system driven by joule heating at high latitudes [*Blanc and Richmond*, 1980]. There was some indication from orbit 2 of the ROCSAT data that a

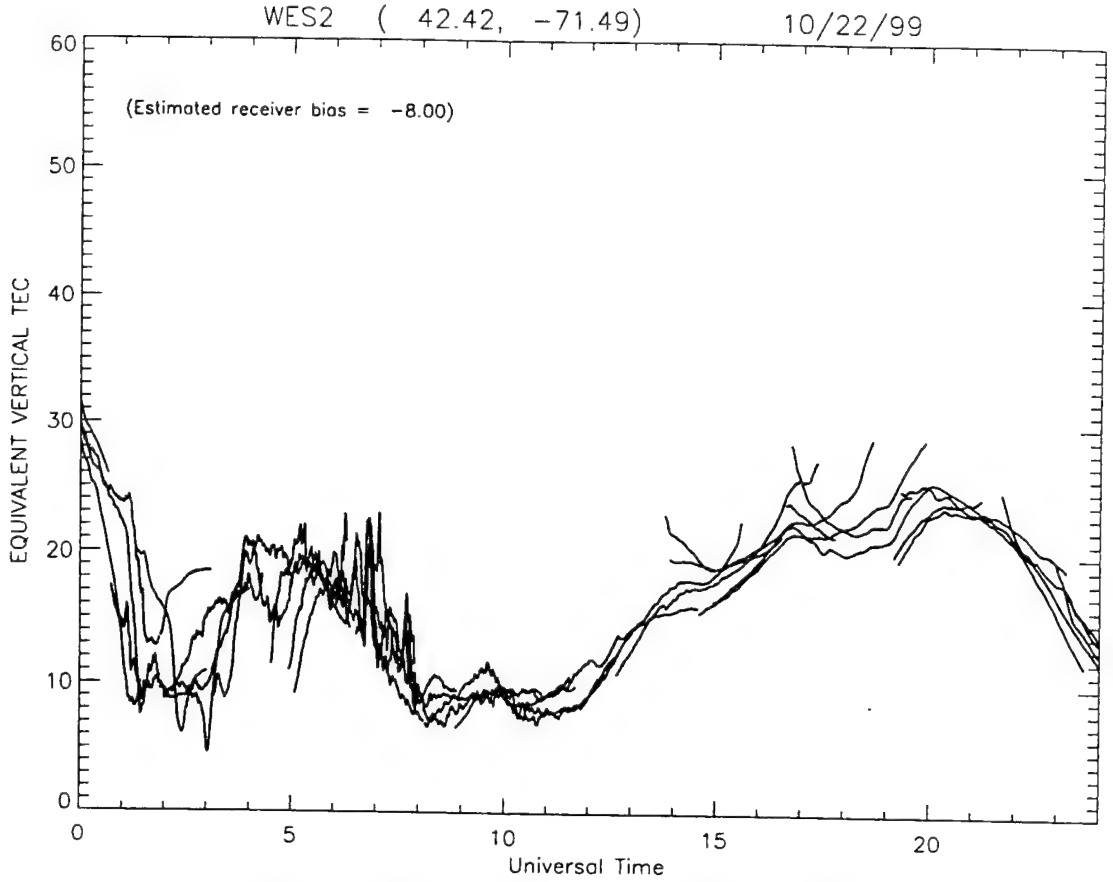

Figure 12. Same as in Figure 3 but for October 22, 1999.

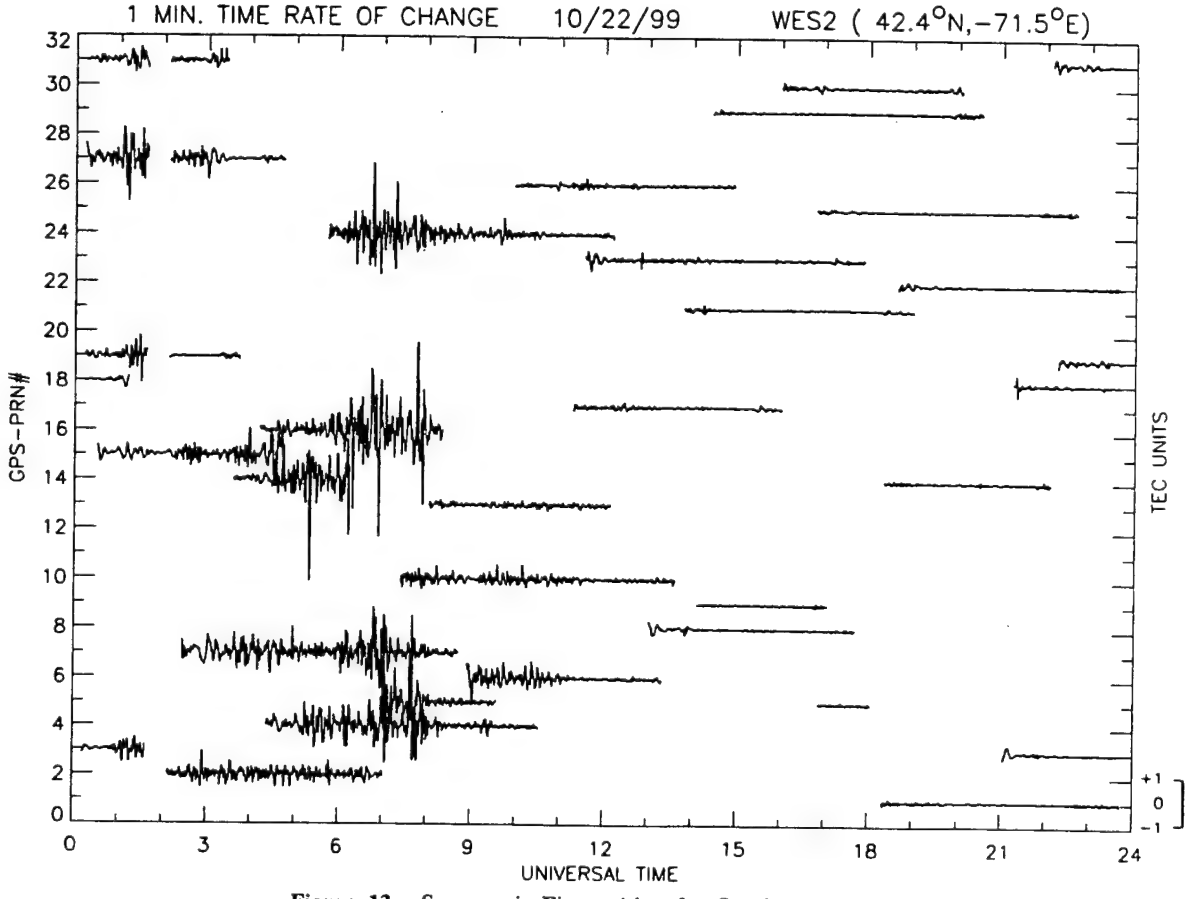

Figure 13. Same as in Figure 4 but for October 22, 1999.

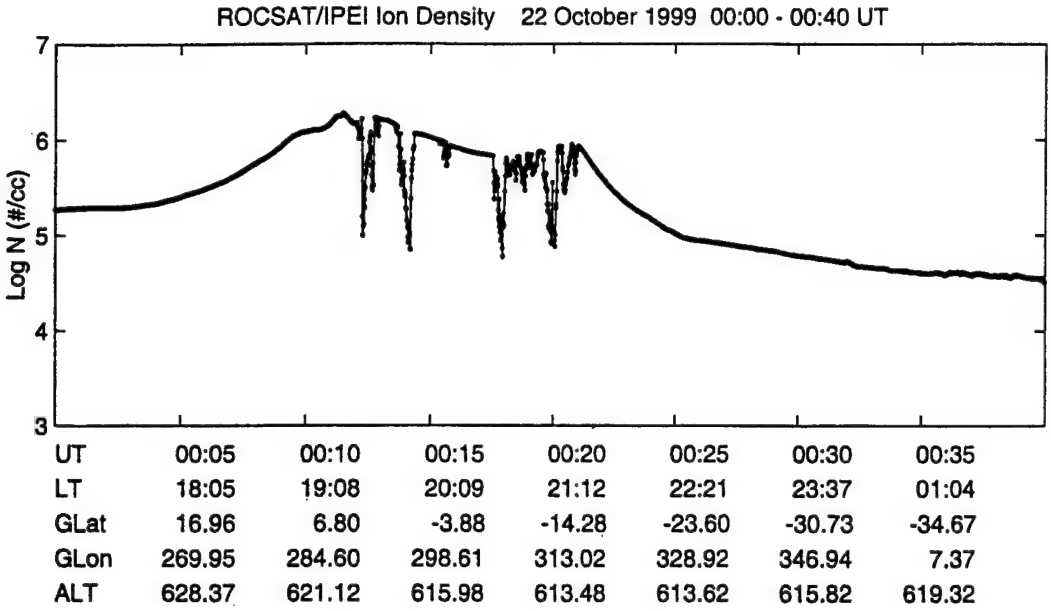

UT	00:05	00:10	00:15	00:20	00:25	00:30	00:35
LT	18:05	19:08	20:09	21:12	22:21	23:37	01:04
GLat	16.96	6.80	-3.88	-14.28	-23.60	-30.73	-34.67
GLon	269.95	284.60	298.61	313.02	328.92	346.94	7.37
ALT	628.37	621.12	615.98	613.48	613.62	615.82	619.32

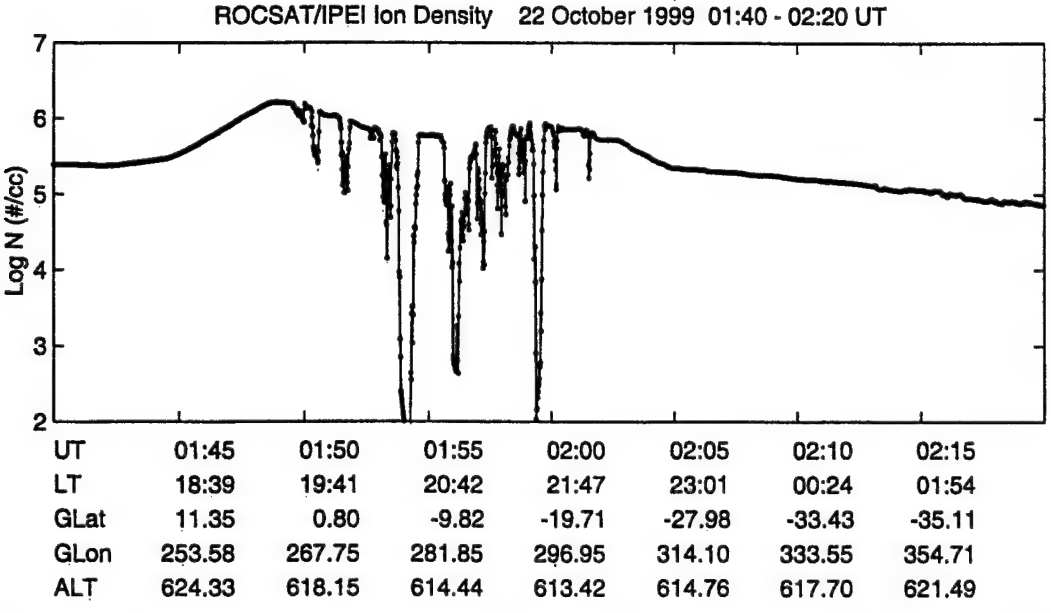

UT	01:45	01:50	01:55	02:00	02:05	02:10	02:15
LT	18:39	19:41	20:42	21:47	23:01	00:24	01:54
GLat	11.35	0.80	-9.82	-19.71	-27.98	-33.43	-35.11
GLon	253.58	267.75	281.85	296.95	314.10	333.55	354.71
ALT	624.33	618.15	614.44	613.42	614.76	617.70	621.49

Figure 14. The total ion density measured by the ROCSAT-1 satellite between 0000–0040 and 0140–0220 UT on October 22, 1999. Wide regions of equatorial irregularity structures extending over 30° of longitude range are seen on both orbits at 600-km altitude.

disturbance dynamo process was gradually getting set up. The disturbance dynamo usually requires a few hours [*Scherliess and Fejer*, 1997] to be established as opposed to the prompt penetration effects both for increasing and decreasing high-latitude convection which occur within tens of minutes of storm intensification [*Spiro et al.*, 1988; *Fejer and Scherliess*, 1995, 1997]. The scintillation structure starting just prior to 0800 UT (0300 LT) in Plate 3a seems to be due to the fresh generation of equatorial irregularities in the postmidnight hours. We base our hypothesis on several aspects of the scintillation data analysis and the simultaneous ROCSAT data shown in Figure 17. The scintillation data provide two reasons for considering the 0800–0900 UT structure to be freshly generated: (1) Scintillations at gigahertz, though small, are definitely observable after many hours of no gigahertz scintillation, and (2) the psds at specific scale lengths, obtained from a combination of the frequency scale of the fast Fourier transform (FFT) spectra and the irregularity drift shown in Plate 3b and depicted in Plate 3c (plotted on log scale), show large amplitudes. In particular, the psds at 500, 250, and 125 m

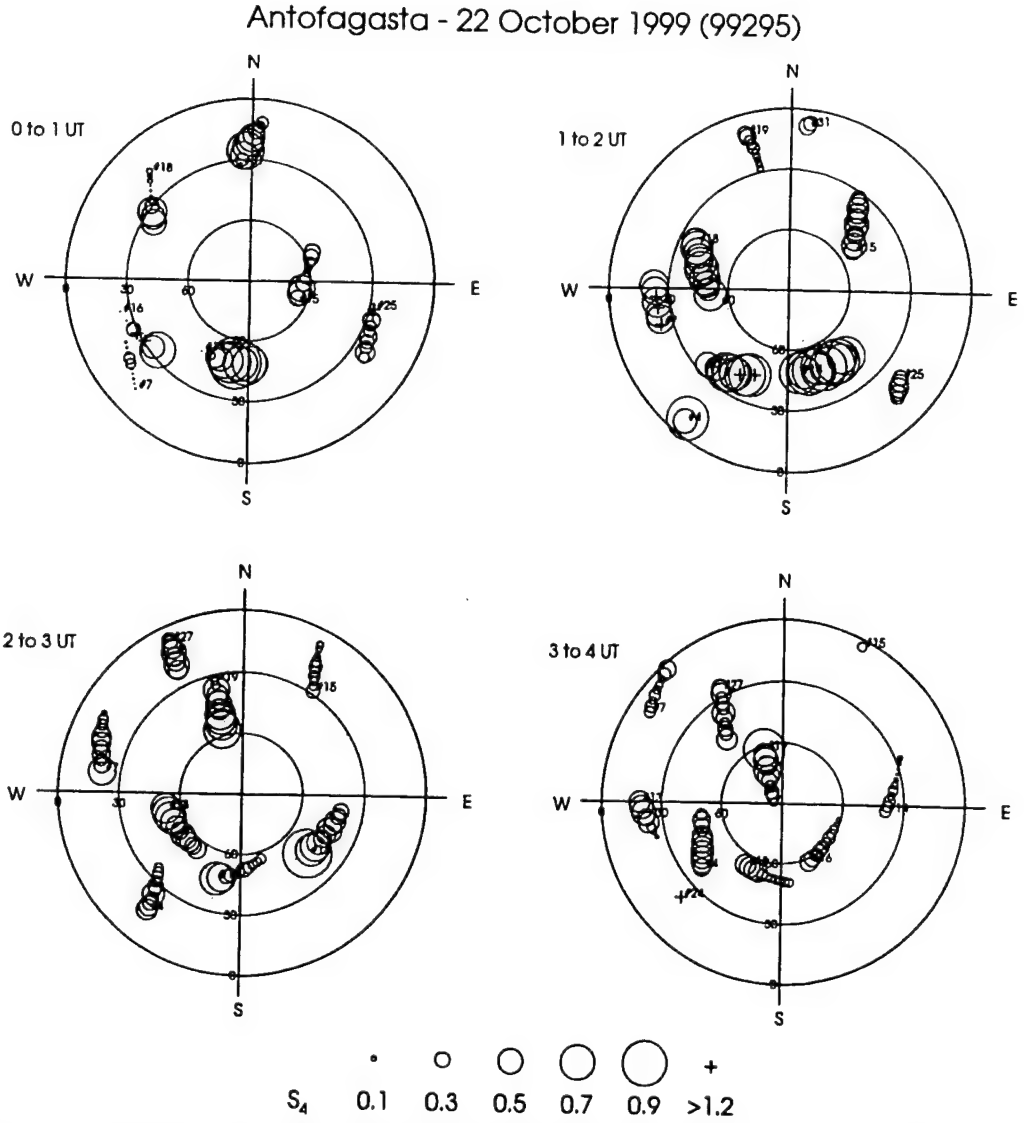

Figure 15. Hourly polar plots of the position and scintillation levels, plotted at 5-min intervals, of all GPS links tracked by the station at Antofagasta, Chile, on October 22, 1999, between 0000 and 0400 UT. Circle size corresponds to S4 level as shown in the legend. Pseudorandom noise (PRN) numbers are plotted at the initial satellite position. The large concentric circles denote elevation angles of 60°, 30°, and 0°. Between 0100 and 0200 UT, intense levels of scintillation are seen on four satellites simultaneously to the south and west of the station.

become suddenly enhanced. This psd behavior is similar to the scintillation characteristics early in the evening when only freshly generated irregularities are observed.

The corresponding ROCSAT data are shown in Figure 17. The irregularity structures between 0820 and 0830 UT are in the Hawaiian sector, and we will discuss that aspect later when trying to determine a westward boundary for the equatorial irregularities. The other structure near 0850 UT (corresponding to 0335 LT) embraces the field line connected to the scintillation ray path from South America and actually passes to the south of Antofagasta. *Yeh et al.* [2001], on the basis of positive correlation of density depletion and enhanced eastward electric field of 1–2 mV m^{-1} resulting from the in-phase contributions of the prompt penetration magnetospheric (due to a sudden northward turning of the IMF) and the long-lasting ionospheric disturbance dynamo electric fields, argue for fresh generation for this large irregularity structure, and we concur on the basis of scintillation characteristics. We shall also discuss these findings in section 4 in more global terms.

As we did for the September 22–23, 1999, magnetic storm, we would like to provide some eastern and western boundaries for equatorial irregularities observed during the October 22 storm. In this case the ROCSAT-1 data are extremely helpful in establishing both eastward and westward boundaries. Plate 4 depicts eight successive orbits on ROCSAT-1, at least five of which showed equatorial irregularities in the early evening generation phase. The portion of the orbits, which are in bold, both yellow and blue show the regions of irregularities. The actual density data showing the presence of irregularities for orbits 1, 2, and 6 have been shown in Figures 14 and 17. It is interesting to note from the LT attached to the first six orbits at irregularity onset that the ROCSAT-1 satellite detected irregularities between 1852 and 1936 LT except for orbit 3. This indicates that, by and large, the satellite must have inter-

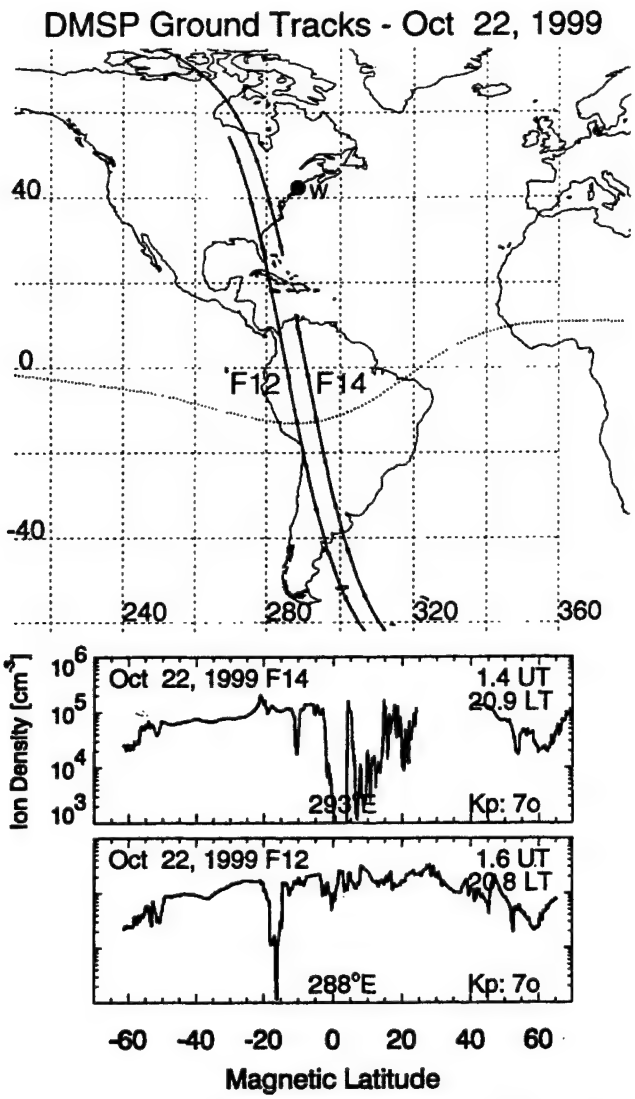

Figure 16. The ion density data at 840 km for the DMSP F12 and F14 orbits (middle and bottom panels) on October 22, 1999, and their orbital tracks (top panel). Wide regions of equatorial irregularities and the existence of the midlatitude trough at ~50° with density enhancement poleward of the trough are clearly visible on both satellites particularly in the Northern Hemisphere.

cepted freshly generated irregularities. While orbits 1 and 2 occurred during the 0000–0200 UT period of intensifying SYM-H (or *Dst*), orbits 4–6 occurred during the second intensification between 0400 and 0600 UT and continued into the time when SYM-H < −200 nT up to ~0900 UT. Thus, on the basis of Plate 4, we find that the equatorial irregularities for this magnetic storm were generated over longitudes ranging between ~170°E and 315°E. It is extremely tempting, as in the case of the September 22–23, 1999, storm, to associate the belt of longitudes where *E* region sunset occurred during times of rapidly increasing negative *Dst* and *Dst* minimum phase as the ones affected by a prompt penetration of magnetospheric electric field into equatorial latitudes. In addition, we found at least one region of probable fresh generation of irregularities at 0300 LT in the South American sector (between 235° and 300°E) that was a good candidate for being caused by the effects of the ionospheric disturbance dynamo perhaps in conjunction with prompt penetration effects due to the northward turning of the IMF as shown in Figure 1 of *Yeh et al.* [2001].

It is very encouraging to note that other ground- and space-based data sets are all consistent with the findings based on ROCSAT-1. For instance, the IGS data for Ascension Island, Malindi, Diego Garcia, Manila, Guam, and Kwajalein showed no activity; that is, no TEC fluctuations were seen, while significant activity was observed at Arequipa, Santiago, and Easter Island. The DMSP F12, F13, and F14 satellite overflights were also consistent with the ROCSAT-1 data presented in Plate 4. Later orbits of ROCSAT-1, namely, orbits 7–12 between 1030 and 1725 UT (orbits 7 and 8 were plotted in Plate 4), all showed smaller-amplitude density irregularities at later local times (0400–0900 LT) but all within the range of longitudes between ~170° and 315°E. Many of these orbits passed through the South American sector and are consistent with the scintillation observations which showed continued activity between 0010 and 0910 UT and thereafter with breaks up to 1400 UT.

4. Summary and Discussion

We have studied the ionospheric effects of two major equinoctial magnetic storms (*Dst* < −150 nT) near solar maximum (smoothed sunspot number ~150) by considering the scintillation and TEC data from some middle-latitude stations which form part of the IGS network within the United States. We found that the prompt penetration of magnetospheric electric fields caused TEC increases, followed by rapid TEC decreases related to the equatorward motion of the midlatitude trough. These effects were enhanced if the rapid *Dst* intensifications took place in the afternoon sector near dusk. The equatorward motion of the trough was accompanied by TEC fluctuations, some as large as ±5 TEC units min^{-1}, and saturated 250-MHz scintillations which may impact the GPS-based navigation system called WAAS and UHF communication links. In its simplest form, the effects of the prompt penetration of electric fields could be traced all the way to the magnetic equator and seemed to be confined to the range of longitudes for which the sunset times (probably at *E* region heights) coincided with the times of storm intensifications and its maximum phase. Thus, with the study of these two storms, one (in September 1999) for which the storm development and recovery was short and in the 2200–0100 UT time frame, a narrow swath of ~60° in the South American and South Atlantic longitudes was affected. The other one (in October 1999) had a much longer development and recovery in the 0000–0900 UT hours and affected a much wider region extending over almost 145° of longitude in the South American and Pacific sectors. Thus extreme variability in irregularity occurrence at particular sites is often encountered during magnetic storms as has been reported by many authors [*Aarons et al.*, 1997; *Abdu et al.*, 1995, and references therein]. Because of the great variety of data types and sites used and different types of effects observed on communication and navigation systems, we provide a summary of our findings and references to the relevant diagrams in Tables 1a and 1b to help the reader.

It should be emphasized that equinox solar maximum conditions are conducive to equatorial irregularity generation at all longitudes during magnetically quiet times (see the review by *Basu and Basu* [1985, and references therein]). Further, general morphological studies based on *Kp* also indicate that

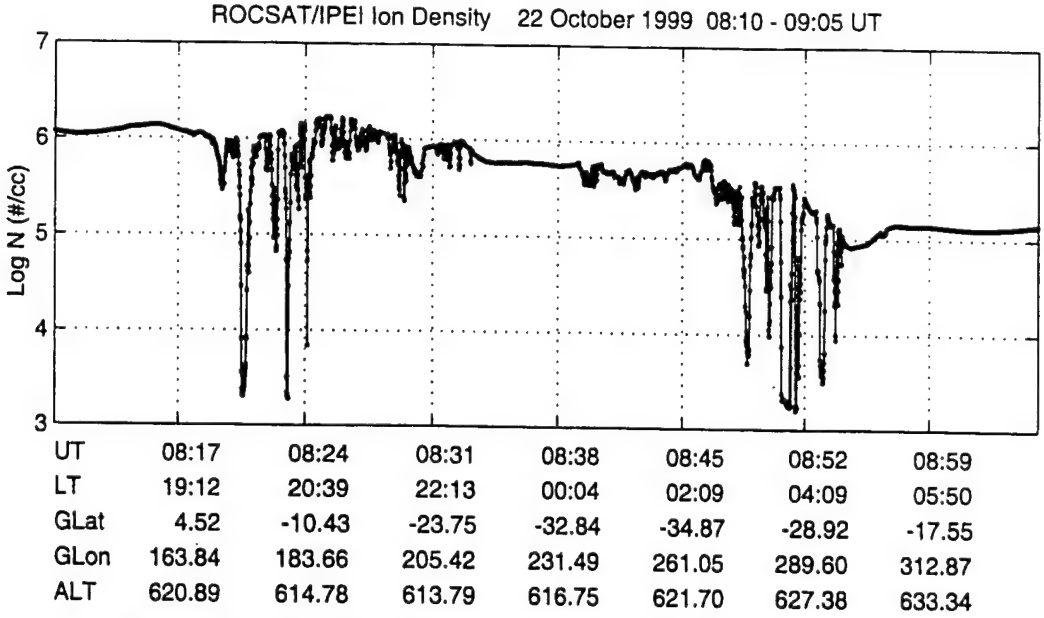

Figure 17. ROCSAT-1 total ion density data at 600 km between 0810 and 0905 UT on October 22, 1999. The irregularity structure near 0820 UT is in the Hawaiian sector whereas that near 0850 UT intersects the magnetic field lines going through the Ancon and Antofagasta stations.

scintillations tend to decrease with high *Kp* in the early evening hours [*Groves et al.*, 1997]. There is evidence from Jicamarca radar measurements for postmidnight irregularity generation during enhanced geomagnetic activity [*Fejer et al.*, 1999]. However, these times have much lower *F* region density so that irregularities, even if they are present, cannot cause intense scintillations in the gigahertz range. Our results, albeit limited to only two equinox storms, show that the equatorial irregularities may be enhanced or inhibited depending on the UT of storm intensification and length of the main phase. A recent paper by *Huang et al.* [2000] has pointed out the presence of equatorial bubbles during the initial and main phase of magnetic storms. In our discussion, in the interest of clarity, we have mainly considered the effect of the prompt penetration of electric fields of magnetospheric origin into low latitudes primarily during the increasing phase of the cross polar cap potential associated with the southward turning of the IMF and the intensification of the ring current. We have briefly mentioned the later time effects, due to the northward turning of the IMF and the more gradual onset of the ionospheric disturbance dynamo. In these two particular cases even the postmidnight events occurred within the region affected by the prompt penetration in the early evening hours. In a study of the May 23–24, 1998, great storm event, *Aarons et al.* [1999] had found a very longitude limited equatorial disturbance in the postmidnight phase that the authors attributed to the disturbance dynamo.

Our experimental findings at equatorial latitudes are generally consistent with the model predictions of the short-lived prompt penetration of electric fields both for increased and decreased magnetospheric convection [*Fejer and Scherliess*, 1997] and the more long-lived disturbance dynamo fields [*Scherliess and Fejer*, 1997] developed on the basis of Jicamarca radar measurements. These authors have used a linear relationship between the cross polar cap potential and AE, the auroral electrojet index [*Ahn et al.*, 1992], for the development of their empirical models. We have used the variation in the 1-min SYM-H index (which closely approximates the hourly *Dst* index) as the indicator for the prompt penetration of electric fields. Our results show that for the case of well-identified major magnetic storms during the initial phase, the time variation of the SYM-H index can effectively track the effects due to this type of prompt penetration of electric fields on communication and navigation systems operating at middle and equatorial latitudes. For the disturbance dynamo effects, however, the AE index during such large magnetic storms is probably a more appropriate measure of the energy input into high latitudes. For the September and October storms discussed in this paper the AE index increase and SYM-H decrease occurred in concert, making it difficult to distinguish between the efficacy of the two indices as a proxy for the cross polar cap potential. However, for the case of the July 15, 2000, superstorm, the AE increase occurred several hours prior to the SYM-H decrease due to ring current development. In that case the midlatitude and equatorial impacts due to prompt penetration of the magnetospheric electric field in the initial phase were still better ordered by variations in the SYM-H index which seemed to be taking place in an environment affected by the disturbance dynamo [*Foster et al.*, 2000; *Basu et al.*, 2001]. The effects on systems of these prompt penetration fields in the dusk sector, particularly during solar maximum, are large enough to merit a serious modeling effort for this magnetosphere-ionosphere coupled phenomenon. Indeed, such modeling efforts are underway to calculate the prompt penetration electric field from model results of the stormtime ring current [*Ridley and Liemohn*, 2001]. It is encouraging to note that in this modeling effort the magnitude of the penetration electric field is related to Dst^*, a solar wind pressure corrected *Dst* index [*Kozyra et al.*, 1998].

The prompt penetration of magnetospheric electric fields into the midlatitude ionosphere induces variations in TEC that may adversely affect the performance of navigation systems. *Garcia et al.* [2000] have documented a similar case at Arecibo, Puerto Rico, where GPS TEC perturbations were observed in

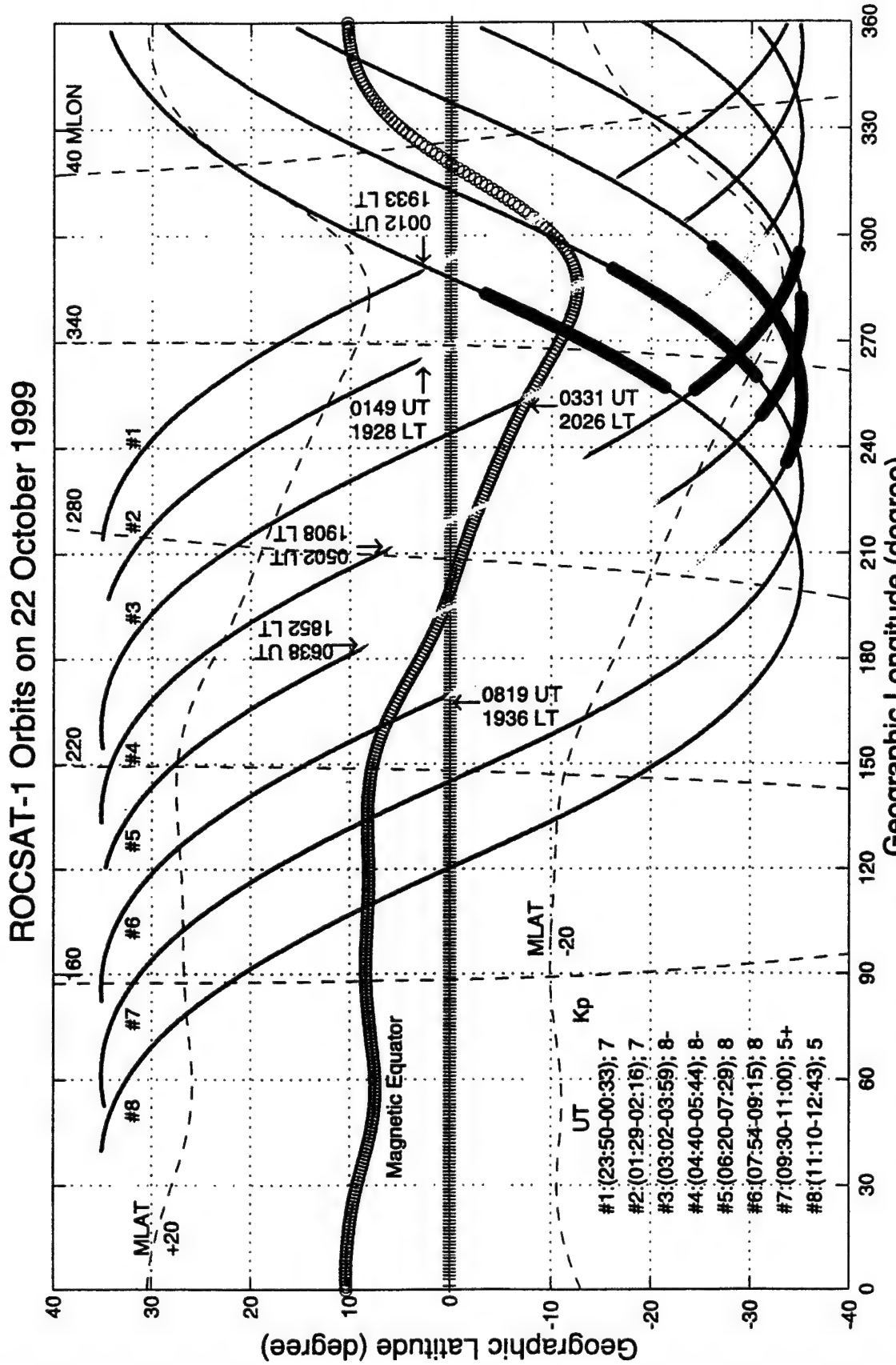

Plate 4. Equatorial portions of the first eight orbits of ROCSAT-1 between 0000 and 1200 UT on October 22, 1999. The thick yellow and blue lines on the orbits indicate the presence of density irregularities at 600 km. The LT at the onset of irregularities for the first six orbits is indicated on the diagram. These six orbits covered the range of longitudes where a fresh generation of equatorial irregularities was seen during the early and main phase of the October 22, 1999, magnetic storm. The thick blue lines show irregularities in the postmidnight phase.

Table 1a. September 22, 1999, $Dst_{min} \sim -167$ nT at 2400 UT, $(dDst/dt)_{max} \sim 75$ nT h^{-1} Between 2200 and 2300 UT[a]

Ionospheric Effects	Observation	Remarks
Prompt effect at midlatitudes		
Large (~km s^{-1}) westward (sunward) convection velocity and increase of hmF_2 and TEC between 2100 and 2200 UT (1600–1700 LT)	DMSP F13 and F14; Millstone Digisonde; IGS GPS RX	magnetospheric E field penetration before sunset with northward and eastward components (Figure 2, Plate 1, and Figures 3 and 5)
Increase of hmF_2; and precipitous decrease of NmF_2 and TEC between 2210 and 2245 UT (1710–1745 LT)	Digisonde; IGS GPS RX	trough moves equatorward (Figures 3 and 5)
Impulsive 250-MHz scintillation and GPS phase fluctuation onset between 2210 and 2240 UT (1710–1740 LT)	Hanscom scintillation RX; IGS GPS RX	plasma instabilities associated with trough gradient cause electron density irregularities with scale lengths of tens of kilometers to tens of meters (Figures 1 and 4)
Prompt effect at equatorial latitudes		
Scintillation at 250 MHz, plasma bubbles, and GPS phase fluctuation; all between 15°W and 73°W	Ancon scintillation RX; South American GPS network; DMSP F12 and F14; global IGS GPS RX	prompt penetration of eastward E field over longitude sector for which early evening period corresponds to the time of rapid Dst (SYM-H) variations; equatorial anomaly development and plasma instability induced topside irregularities (Figures 6–9)
Postmidnight effects at equatorial latitudes		
Postmidnight scintillation in South Atlantic	Ancon and Ascension scintillation RX	possible disturbance dynamo-induced irregularity formation over longitude sector affected by prompt penetration E field

[a]TEC, total electron content; IGS, International GPS Service for Geodynamics; GPS, Global Positioning System; RX, Receiver.

conjunction with airglow enhancements during a high geomagnetic activity period. Our study has shown that the LT of penetration of the electric field dictates the magnitude of the system impacts. A specific occurrence at local dusk is the equatorward motion of the midlatitude trough that, in turn, creates plasma instabilities driven by the gradient. If one assumes that in addition to the large sunward (or westward) flow seen in Plate 1, the plasma is moving equatorward in the neutral frame of reference, then this geometry is consistent with the requirements of the gradient drift instability (see the review by *Tsunoda* [1988]). Sometimes these equatorward and westward motions bring auroral blobs into the erstwhile midlatitude ionosphere, the trailing edges of which are also seen to cause intense 250-MHz amplitude scintillations and TEC fluctuations at GPS frequencies. This unexpected TEC increase and its fluctuations in the midnight time frame caused the largest errors in the WAAS algorithms in the continental United States. Needless to say, the morphology of such trough-wall gradients and auroral blob structures has to be studied using a large data-base such as the one existing at Millstone Hill [*Vo and Foster*, 2001] so that predictive schemes may be developed for use during magnetic storms.

Finally, we come to a consideration of the effects of penetrating electric fields on the equatorial ionosphere. At the recent Equatorial Aeronomy Symposium in Antalya, Turkey, in May 2000, there was consensus among the participants that the topic is still one of the major unknowns in the field. Most of our information to date has come from the modeling efforts undertaken by B. G. Fejer and L. Scherliess (see references quoted earlier) based on vertical drift measurements by the Jicamarca radar. These single-point measurements have been skillfully interpreted by these authors to provide LT and storm time coverage at all longitudes for both the prompt penetration (for convection increase and decrease) fields and the disturbance dynamo. We took a more global approach in an attempt to link a UT-driven phenomenon (namely, ring current development) with one dependent on LT, namely, E region sunset, creating conductivity gradients at specific locations. For the two storms discussed here and the July 15, 2000, storm [*Basu et al.*, 2001], we find that equatorial irregularities are generated in the prompt penetration of the development phase at longitudes for which E region sunset is observed during a fast change in the SYM-H index on the order of 50 nT h^{-1}, and SYM-H achieves values in the range of about -150 nT or smaller. Obviously, many more magnetic storms have to be studied under different seasonal and sunspot cycle conditions to test this hypothesis. If it holds, then it could be introduced as a nowcasting tool in equatorial scintillation prediction.

Both these storms provided evidence for the fresh generation of irregularities in the post-midnight time frame. This can be attributed to the disturbance dynamo generated eastward electric field. Both storms also showed a prompt northward turning of the IMF indicating storm recovery, which could have provided a short-lived in-phase contribution to the disturbance dynamo effects. However, for the September 1999 storm the northward turning was not at the appropriate time whereas for the October storm the two effects seemed to have provided an in-phase contribution in the postmidnight irregularity generation. What is quite interesting is that the postmidnight event for both storms occurred within a part of the longitude range affected by prompt penetration in the early evening (generation) period. The same was found to be true for the July 15, 2000, storm [*Basu et al.*, 2001]. If this holds up for more storm studies, it may indicate that the background ionosphere which turned unstable earlier in the evening had a greater likelihood of becoming unstable again in the postmidnight hours. However, since the most favorable time for this joint effect is near 0300 LT [*Scherliess and Fejer*, 1997], the impacts on commu-

Table 1b. October 22, 1999, $Dst_{min} \sim -231$ nT at 0700 UT, $(dDst/dt)_{max} \sim 45$ nT h^{-1} During 0000–0200 and 0400–0600 UT

Ionospheric Effects	Observation	Remarks
Prompt effect at midlatitudes		
250-MHz scintillation onset at 0120 and 0440 UT	Hanscom scintillation RX	scintillation structures due to two periods of penetration *E* fields; monitored by two periods of fast *Dst* (SYM-H) decreases (Figure 10)
NmF_2 and TEC fast decrease at 0000–0300 UT (1900–2200 LT)	Millstone Digisonde; IGS GPS RX	trough moves equatorward causes first scintillation structure (Figures 10–12)
NmF_2 and TEC increase during 0400–0700 UT (2300–0200 LT)	Digisonde; IGS GPS RX; DMSP F-12 and F-14	auroral blob causes TEC increase; second scintillation event observed (Figures 10–12 and 16)
GPS phase fluctuation between 0500 and 0800 UT	IGS GPS RX	trailing edge of blob structured; WAAS parameter GIVE exceeds 6 m during TEC fluctuation (Figures 12 and 13 and Plate 2)
Prompt effect at equatorial latitudes		
250-MHz and *L* band scintillation onset at 0010 UT (1910 LT)	Ancon scintillation RX; ROCSAT-1	near-simultaneous plasma bubble generation over 30° longitude interval (Figure 7, Plate 3, and Figure 14)
Strong GPS amplitude scintillation near crest of equatorial anomaly	Antofagasta GPS RX; ROCSAT-1	plasma bubbles extend to equatorial anomaly crest (Figures 14 and 15)
Irregularities in the topside detected over a longitude interval of 170°E–315°E in the local evening hours	ROCSAT-1 satellite	prompt penetration of eastward *E* field over longitude sector for which early evening period corresponds to the time of rapid *Dst* (SYM-H) variations (Plate 4)
Topside plasma bubbles cover ±20° MLAT	DMSP F12 and F14	plasma bubbles attain high altitudes (>840 km) over the magnetic equator (Figure 16)
Postmidnight effects at equatorial latitudes		
Fresh generation of irregularities and scintillation at 0800 UT (0300 LT) with westward drift	Ancon scintillation RX; ROCSAT-1	IMF *Bz* northward turning and ionospheric disturbance dynamo induced irregularity generation and westward drift (Plate 3 and Figure 17)

nication and navigation systems may be rather limited as the background densities are much lower at that local time.

Acknowledgments. Sunanda Basu gratefully acknowledges a six-month professional development leave from the National Science Foundation that made this study possible. She thanks the Air Force Research Laboratory at Hanscom AFB, MA, and the National Central University (NCU) at Chung-Li, Taiwan, for hosting her during this period. Santimay Basu also thanks the NCU for its hospitality. The efforts of J. U. Kozyra and D. Webb in providing space weather information through the International Space Weather Clearinghouse Web page are much appreciated. We thank J. W. Wright for his assistance with the Digisonde data analysis. The work at AFRL was supported by AFOSR task 2311AS. The work at Boston College was supported by NSF grant ATM-9819912 and AFRL contract F19628-97-C-0094. The work at NCU was supported by NSC (ROC) grant NSC 89-NSPO (A)-PDD-008-STP01.

Janet G. Luhmann thanks the referees for their assistance in evaluating this paper.

References

Aarons, J., The longitudinal morphology of equatorial *F*-layer irregularities relevant to their occurrence, *Space Sci. Rev.*, *63*, 209, 1993.

Aarons, J., and R. S. Allen, Scintillation boundary during quiet and disturbed magnetic conditions, *J. Geophys. Res.*, *76*, 170, 1971.

Aarons, J., R. S. Allen, and H. E. Whitney, Observations of scintillations of two satellite beacons near the boundary of the irregularity region, *Planet. Space Sci.*, *20*, 965, 1972.

Aarons, J., M. Mendillo, and R. Yantosca, GPS phase fluctuations in the equatorial region during sunspot minimum, *Radio Sci.*, *32*, 1535, 1997.

Aarons, J., M. Mendillo, and B. Lin, The great magnetic storm of May 1998 and its effect on phase fluctuations in the auroral and equatorial regions, paper presented at Ionospheric Effects Symposium, Off. of Nav. Res., Arlington, Va., 1999.

Abdu, M. A., I. S. Batista, G. O. Walker, J. H. A. Sobral, N. B. Trivedi, and E. R. de Paula, Equatorial ionospheric electric fields during magnetospheric disturbances: Local time/longitudinal dependencies from recent EITS campaign, *J. Atmos. Terr. Phys.*, *57*, 1065, 1995.

Ahn, B.-H., Y. Kamide, H. W. Kroehl, and D. J. Gorney, Cross polar potential difference, auroral electrojet indices, and solar wind parameters, *J. Geophys. Res.*, *97*, 1345, 1992.

Basu, S., and A. Das Gupta, Latitude variation of electron content in the equatorial region under magnetically quiet and active conditions, *J. Geophys. Res.*, *73*, 5599, 1968.

Basu, S., Su. Basu, J. Aarons, J. P. McClure, and M. C. Cousins, On the co-existence of km- and m-scale irregularities in the nighttime equatorial *F*-region, *J. Geophys. Res.*, *83*, 4219, 1978.

Basu, S., Su. Basu, J. LaBelle, E. Kudeki, B. J. Fejer, M. C. Kelley, H. E. Whitney, and A. Bushby, Gigahertz scintillations and spaced receiver drift measurements during Project Condor equatorial *F*-region rocket campaign in Peru, *J. Geophys. Res.*, *91*, 5526, 1986.

Basu, S., et al., Scintillations, plasma drifts, and neutral winds in the equatorial ionosphere after sunset, *J. Geophys. Res.*, *101*, 26,795, 1996.

Basu, S., K. M. Groves, J. M. Quinn, and P. Doherty, A comparison of TEC fluctuations and scintillations at Ascension Island, *J. Atmos. Terr. Phys.*, *61*, 1219, 1999.

Basu, S., Su. Basu, K. M. Groves, H.-C. Yeh, S.-Y. Su, F. J. Rich, and P. J. Sultan, Response of the equatorial ionosphere in the South Atlantic region to the great magnetic storm of July 15, 2000, *Geophys. Res. Lett.*, *28*, 3577, 2001.

Basu, Su., VHF ionospheric scintillations at $L = 2.8$ and formation of stable auroral red arcs by magnetospheric heat conduction, *J. Geophys. Res.*, *79*, 3155, 1974.

Basu, Su., and S. Basu, Equatorial scintillations: Advances since ISEA-6, *J. Atmos. Terr. Phys.*, *47*, 753, 1985.

Basu, Su., E. MacKenzie, S. Basu, H. C. Carlson, D. A. Hardy, F. J. Rich, and R. C. Livingston, Coordinated measurements of low-energy electron precipitation and scintillations/TEC in the auroral oval, *Radio Sci.*, *18*, 1151, 1983a.

Basu, Su., S. Basu, J. P. McClure, W. B. Hanson, and H. E. Whitney, High resolution in situ data of electron densities and VHF/GHz scintillations in the equatorial region, *J. Geophys. Res.*, *88*, 403, 1983b.

Basu, Su., S. Basu, E. MacKenzie, W. R. Coley, J. R. Sharber, and W. R. Hoegy, Plasma structuring by the gradient-drift instability at high latitudes and comparison with velocity-shear driven processes, *J. Geophys. Res.*, *95*, 7799, 1990.

Bhattacharyya, A., T. L. Beach, S. Basu, and P. M. Kintner, Nighttime equatorial ionosphere: GPS scintillations and differential carrier phase fluctuations, *Radio Sci.*, *35*, 209, 2000.

Blanc, M., and A. D. Richmond, The ionospheric disturbance dynamo, *J. Geophys. Res.*, *85*, 1669, 1980.

Briggs, B. H., and I. A. Parkin, On the variation of radio star and satellite scintillation with zenith angle, *J. Atmos. Terr. Phys.*, *25*, 339, 1963.

Buonsanto, M., Ionospheric storms: A review, *Space Sci. Rev.*, *61*, 193, 1999.

Buonsanto, M. J., M. Mendillo, and J. A. Klobuchar, The ionosphere at $L = 4$: Average behavior and response to geomagnetic storms, *Ann. Geophys.*, *35*, 15, 1979.

Burke, W. J., et al., Electrodynamics of the inner magnetosphere observed in the dusk sector by CRRES and DMSP during the magnetic storm of June 4–6, 1991, *J. Geophys. Res.*, *103*, 29,399, 1998.

Dehel, T., K. Pham, and J. Sheftic., National Satellite Test Bed (NSTB) observations of the effects of ionospheric storms on a prototype wide area augmentation system, paper presented at National Technical Meeting, Inst. of Navig., San Diego, Calif., 1999.

Doherty, P., E. Raffi, J. A. Klobuchar, and M. B. El-Arini, Statistics of time rate of change of ionospheric range delay, paper presented at 7th International Technical Meeting, Inst. of Navig., Salt Lake City, Utah, 1994.

Evans, J. V., The causes of storm-time increases of the *F*-layer at midlatitudes, *J. Atmos. Terr. Phys.*, *35*, 593, 1973.

Fejer, B. G., and L. Scherliess, Time dependent response of equatorial ionospheric electric fields to magnetospheric disturbances, *Geophys. Res. Lett.*, *22*, 851, 1995.

Fejer, B. G., and L. Scherliess, Empirical models of storm time equatorial zonal electric fields, *J. Geophys. Res.*, *102*, 24,047, 1997.

Fejer, B. G., L. Scherliess, and E. R. dePaula, Effects of the vertical plasma drift velocity on the generation and evolution of equatorial spread *F*, *J. Geophys. Res.*, *104*, 19,859, 1999.

Foster, J. C., Storm time plasma transport at middle and high latitudes, *J. Geophys. Res.*, *98*, 1675, 1993.

Foster, J. C., and J. Aarons, Enhanced antisunward convection and *F* region scintillations at mid-latitudes during storm onset, *J. Geophys. Res.*, *93*, 11,537, 1988.

Foster, J. C., and F. J. Rich, Prompt midlatitude electric field effects during severe geomagnetic storms, *J. Geophys. Res.*, *103*, 26,367, 1998.

Foster, J. C., S. Basu, Su. Basu, A. J. Coster, and F. J. Rich, Subauroral ionospheric disturbance and space weather effects during the July 15–16, 2000 geomagnetic storm, *Eos Trans. AGU*, *81*(48), Fall Meet. Suppl., SH62A-10, 2000.

Garcia, F. J., M. C. Kelley, J. J. Makela, P. J. Sultan, X. Pi, and S. Musman, Mesoscale structure of the midlatitude ionosphere during high geomagnetic activity: Airglow and GPS observations, *J. Geophys. Res.*, *105*, 18,417, 2000.

Gonzales, C. A., M. C. Kelley, R. A. Behnke, J. F. Vickrey, R. Wand, and J. Holt, On the latitudinal variations of the ionospheric electric field during magnetospheric disturbances, *J. Geophys. Res.*, *88*, 9135, 1983.

Groves, K. M., et al., Equatorial scintillation and systems support, *Radio Sci.*, *32*, 2047, 1997.

Hanson, W. B., and R. J. Moffett, Ionization transport effects in the equatorial *F* region, *J. Geophys. Res.*, *71*, 5559, 1966.

Hardy, D. A., L. K. Schmidt, M. S. Gussenhoven, F. J. Marshall, H. C. Yeh, T. L. Shumaker, A. Huber, and J. Pantazis, Precipitating electron and ion detectors (SSJ/4) for the Block 5D/Flights 4-10 DMSP satellites: Calibration and data presentation, *Tech. Rep. AFGL-TR-84-0317*, Air Force Geophys. Lab., Hanscom Air Force Base, Mass., 1984.

Huang, C. Y., W. J. Burke, J. S. Machuzak, L. C. Gentile, and P. J. Sultan, DMSP observations of equatorial plasma bubbles in the topside ionosphere near solar maximum, *Eos Trans. AGU*, *81*(48), Fall Meet. Suppl., SA21A-10, 2000.

Iyemori, T., T. Araki, T. Kamei, and M. Takeda, Mid-latitude geomagnetic indices "ASY" and "SYM" for 1999 (provisional), http://swdcdb.kugi.kyoto-u.ac.jp/aeasy/asy.pdf, World Data Cent. C2 for Geomagn., Kyoto, Japan, 2000.

Kelley, M. C., *The Earth's Ionosphere*, pp. 95–104, Academic, San Diego, Calif., 1989.

Kozyra, J. U., et al., The role of precipitation losses in producing the rapid early recovery phase of the great magnetic storm of February 1986, *J. Geophys. Res.*, *103*, 6801, 1998.

McClure, J. P., W. B. Hanson, and J. F. Hoffman, Plasma bubbles and irregularities in the equatorial ionosphere, *J. Geophys. Res.*, *82*, 2650, 1977.

Mendillo, M., and J. A. Klobuchar, Investigations of the ionospheric *F*-region using multistation total electron content observations, *J. Geophys. Res.*, *80*, 643, 1975.

Mendillo, M., M. D. Papagiannis, and J. A. Klobuchar, Ionospheric storms at midlatitudes, *Radio Sci.*, *5*, 895, 1970.

Ossakow, S. L., Spread-*F* theories: A review, *J. Atmos. Terr. Phys.*, *43*, 437, 1981.

Pi, X., A. J. Mannucci, U. J. Lindqwister, and C. M. Ho, Monitoring of global ionospheric irregularities using worldwide GPS network, *Geophys. Res. Lett.*, *24*, 2283, 1997.

Reinisch, B. W., and H. Xueqin, Automatic calculation of electron density profiles from digital ionograms, 3, Processing of bottomside ionograms, *Radio Sci.*, *18*, 477, 1983.

Rich, F. J., and M. Hairston, Large-scale convection patterns observed by DMSP, *J. Geophys. Res.*, *99*, 3827, 1994.

Ridley, A. J., and M. W. Liemohn, A model-derived storm time asymmetric ring current driven electric field description, *J. Geophys. Res.*, in press, 2001.

Rishbeth, H., and W. B. Hanson, A comment on plasma "pile up" in the *F* region, *J. Atmos. Terr. Phys.*, *36*, 703, 1974.

Scherliess, L., and B. G. Fejer, Storm time dependence of equatorial disturbance dynamo zonal electric fields, *J. Geophys. Res.*, *102*, 24,037, 1997.

Spiro, R. W., R. A. Wolf, and B. G. Fejer, Penetration of high-latitude electric field effects to low latitudes during SUNDIAL 1984, *Ann. Geophys.*, *6*, 39, 1988.

Sugiura, M., and D. J. Poros, Hourly values of equatorial *Dst* for years 1957–1970, *NASA-GSFC Doc. X-645-71-278*, Goddard Space Flight Cent., Greenbelt, Md., 1971.

Tanaka, T., Severe ionospheric disturbances caused by the sudden response of evening subequatorial ionospheres to geomagnetic storms, *J. Geophys. Res.*, *86*, 11,335, 1981.

Tsunoda, R., High-latitude *F*-region irregularities: A review and synthesis, *Rev. Geophys.*, *26*, 719, 1988.

Valladares, C. E., R. Sheehan, S. Basu, H. Kuenzler, and J. Espinoza, The multi-instrumented studies of equatorial thermosphere aeronomy scintillation system: Climatology of zonal drifts, *J. Geophys. Res.*, *101*, 26,839, 1996.

Valladares, C., S. Basu, K. Groves, M. P. Hagan, D. Hysell, A. J. Mazzella Jr., and R. E. Sheehan, Measurement of the latitudinal distributions of total electron content during equatorial spread *F* events, *J. Geophys. Res.*, in press, 2001.

Vo, H. B., and J. C. Foster, A quantitative study of ionospheric density gradients at mid-latitudes, *J. Geophys. Res.*, in press, 2001.

Woodman, R. F., Vertical drift velocities and east-west electric fields at the magnetic equator, *J. Geophys. Res.*, *75*, 6249, 1970.

Woodman, R. F., East-west ionospheric drifts at the magnetic equator, *Space Res.*, *12*, 968, 1972.

Wygant, J., D. Rowland, H. J. Singer, M. Temerin, F. Mozer, and M. K. Hudson, Experimental evidence on the role of the large spatial scale electric field in creating the ring current, *J. Geophys. Res.*, *103*, 29,527, 1998.

Yeh, H.-C., J. C. Foster, F. J. Rich, and W. Swider, Storm-time electric field penetration observed at mid-latitude, *J. Geophys. Res.*, *96*, 5707, 1991.

Yeh, H. C., S. Y. Su, Y. C. Yeh, J. M. Wu, R. A. Heelis, and B. T. Holt, Scientific mission of the IPEI payload on board ROCSAT-1, *Terr. Atmos. Ocean Sci.*, suppl., p. 19, March 1999.

Yeh, H. C., S. Y. Su, and R. A. Heelis, Storm time plasma irregularities in the pre-dawn hours observed by the low-latitude ROCSAT-1 satellite at 600 km altitude, *Geophys. Res. Lett.*, *28*, 685, 2001.

J. Aarons, Center for Space Physics, Boston University, Boston, MA 02215, USA.

S. Basu, T. W. Bullett, K. M. Groves, F. J. Rich, and P. J. Sultan, Space Vehicles Directorate, Air Force Research Laboratory, Hanscom AFB, MA 01731-3010, USA.

Su. Basu, Atmospheric Sciences Division, National Science Foundation, 4201 Wilson Boulevard, Rm. 775, Arlington, VA 22230, USA. (sbasu@nsf.gov)

P. Doherty, E. MacKenzie, and C. E. Valladares, Institute for Scientific Research, Boston College, Chestnut Hill, MA 02467, USA.

S.-Y. Su and H.-C. Yeh, Institute of Space Science, National Central University, Chung-Li, 32054 Taiwan.

(Received February 28, 2001; revised June 15, 2001; accepted June 18, 2001.)